Photosynthetically Active Radiation: Measurement and Modeling

Matti Mõttus[1], Madis Sulev[2], Frédéric Baret[3], Raoul Lopez-Lozano[3], Anu Reinart[2]
[1]Department of Geosciences and Geography, University of Helsinki, Helsinki, Finland
[2]Tartu Observatory, Tõravere, Tartumaa, Estonia
[3]INRA, UMR Environnement Méditerranéen et Modélisation des Agro-Hydrosystèmes, EMMAH, Avignon, France

Article Outline

Glossary

Photosynthetically active radiation (PAR) The part of electromagnetic radiation that can be used as the source of energy for photosynthesis by green plants, measured as PAR irradiance or PPFD.

PAR waveband Spectral region for electromagnetic radiation defined by the wavelength limits of 400–700 nm.

PAR irradiance Radiant flux density, or the radiative energy received by unit surface area in unit time, carried by photons in the PAR waveband.

Photosynthetic photon flux density (PPFD) The number of photons with wavelengths in the PAR waveband passing through unit surface area in unit time; synonymous to PAR quantum flux.

Photosynthetic action spectrum The spectral dependence of photosynthetic productivity per unit absorbed energy, usually plotted in relative units.

IPAR Intercepted PAR, or the amount of incident PAR not directly transmitted to the ground by a vegetation canopy.

APAR Absorbed PAR, the amount of incident PAR absorbed by a vegetation canopy.

fIPAR The fraction of incident PAR not directly transmitted to the ground by a vegetation canopy.

fAPAR The fraction of incident PAR absorbed by a vegetation canopy.

Global PAR The sum of diffuse and direct PAR: total PAR falling on a horizontal surface.

Ideal PAR energy sensor PAR sensor with output proportional to PAR irradiance.

Ideal PAR quantum sensor PAR sensor with output proportional to PPFD.

Spectral error Broadband radiation measurement errors arising from the deviation of the predicted radiation spectrum from the actual one.

Radiative transfer theory (RTT) The mathematical framework for describing the radiation field in an absorbing, scattering, and emitting medium based on radiation beams traveling in straight lines.

Definition of the Subject

In the broad sense, photosynthetically active radiation (PAR) is the part of electromagnetic radiation that can be used as the source of energy for photosynthesis by green plants. Technically, it is defined as radiation in the spectral range from 400 to 700 nm [1, 2]. It is expressed either in terms of photosynthetic photon flux density (PPFD, μmol photons m^{-2} s^{-1}), since photosynthesis is a quantum process, or in terms of photosynthetic radiant flux density (PAR irradiance, W m^{-2}), more suitable for energy balance studies. A fundamental term in the quantification of light used by plants in the photosynthesis process is the fraction of absorbed photosynthetically active radiation (fAPAR) calculated as the ratio of absorbed to total incident PAR in a vegetation canopy. This variable is widely used in vegetation functioning models at a range of spatial scales from the plant to the globe as an indicator of the amount of energy available for photosynthesis [3].

Introduction

Defining PAR

Photosynthetically active radiation (PAR) is commonly defined as electromagnetic radiation in the waveband

between 400 and 700 nm, or 0.400–0.700 μm [1, 2, 4, 5]. The modern definition of PAR arises from the understanding that the measurement system should be based on a single, generalized spectral response curve based on measured data and usable with sufficient accuracy for all practical purposes [6]. This response curve is commonly known as the action spectrum of photosynthetic radiation and is defined as the photosynthetic productivity (measured as CO_2 uptake or production of O_2) of a leaf plotted against the wavelength λ of the incident spectral irradiance I_λ.

In addition to the action spectrum, the efficiency of photosynthesis is often presented as quantum yield: photosynthetic productivity divided by the amount of absorbed photons. Both quantities are plotted in relative units in Fig. 1: the maximum value of the action spectrum and the relative spectral quantum yield are normalized to unity. The action spectrum and relative spectral quantum yield differ (1) in the units used to measure radiation (amount of photons or amount of radiative energy), and (2) whether the incident or absorbed radiation flux is used. Radiation units for monochromatic radiation can be easily converted: the number of photons with wavelength λ and the corresponding spectral irradiance I_λ are connected via the Planck law (see section "Quantifying PAR"). Absorbed radiative energy (or, equivalently, the number of photons) for each wavelength can be obtained from incident energy by multiplying it by the leaf spectral absorptance.

The shape of photosynthetic action spectrum is almost universal [1, 7]. Small variations are due to between-species differences (e.g., differences in the blue and ultraviolet spectral regions have been noted for arboreous and herbaceous plants [7]), differences in development phase, place of growth, water supply, mineral nutrition, incident irradiance, and other locally varying conditions. This is due to all plants containing the same photochemical apparatus based on the same radiation-absorbing pigments like chlorophyll-A, chlorophyll-B, and carotenoids. These pigments also govern the leaf spectral absorption in the PAR waveband. Only at blue wavelengths, a considerable absorption by non-photosynthetic pigments can be observed [7].

The photosynthetic action spectrum does not decrease to zero at the limits of the PAR waveband

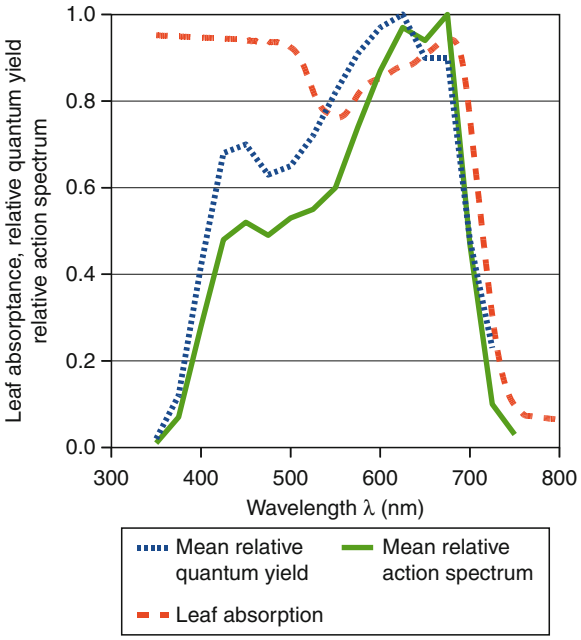

Photosynthetically Active Radiation: Measurement and Modeling. Figure 1
The mean spectral absorption of green leaves (average of measurements in Estonia for common local broad-leaf tree species in 2006) together with the action spectrum of PAR and the relative spectral quantum yield of photosynthesis for field-grown plants (Tables IV and VI in [1])

since the change in photosynthetic potential at 400 and 700 nm is fast but not abrupt. Thus, to exactly measure the true photosynthetic potential of incident radiation, one would need to calculate the incident photon flux density weighed by the relative photosynthetic action spectrum for all wavelengths where the action spectrum is not zero, between 360 and 760 nm. The quantity thus obtained is known as the yield photon flux (YPF) [8].

However, to simplify calculations and measurements, the limits of the PAR waveband have been set to 400 and 700 nm by convention, ignoring the relatively small photosynthetic contribution of photons with wavelengths below 400 nm or above 700 nm. Additionally, the true action spectrum and the spectral composition of incident radiation are generally not used, except for most detailed calculations. Instead, an integral value known as PPFD (section "Quantifying PAR")

is applied (both as a measured value and a theoretical driving force behind photosynthesis in mathematical models) as an adequate descriptor of the photosynthesis-inducing capability of incident radiation under most illumination conditions [2]. The small improvement achievable by using the detailed curve in Fig. 1 does not outweigh the increase in technical and computational complexities.

The radiation incident on a plant canopy arrives as direct and diffuse fluxes. The direct flux is formed by photons having passed through the atmosphere unscattered, whereas the diffuse flux consists of photons scattered by air molecules, aerosol particles, or clouds. As the two fluxes penetrate a vegetation canopy, photons hitting the leaves and other plant elements are intercepted, that is, removed from the incident fluxes. This photon flux hitting plant elements is known as the intercepted PAR flux and denoted with IPAR. Only the intercepted fraction of radiation, or IPAR, constitutes a potential energy source for photosynthesis. However, not all of this potential is realized: a fraction of radiation is always reflected or transmitted by the intercepting element. After being transmitted or reflected, photons may eventually escape the vegetation canopy without any contribution to photosynthesis.

Only photons actually absorbed by the canopy constitute the absorbed PAR (APAR) flux and may be used for photosynthesis. It usually holds that APAR < IPAR and a constant coefficient, APAR = 0.85 IPAR, has been proposed for radiation use efficiency calculations [9] based on the work presented in [10]. Both IPAR and APAR are often expressed in relative units as fractional IPAR (fIPAR) and fractional APAR (fAPAR), respectively, by dividing the relevant quantity by the incident PAR flux. These fractional quantities are expressed as numbers between 0 (no interception or no absorption) and 1 (total interception or total absorption). More details on calculating and measuring APAR, fAPAR, and fIPAR are given in section "PAR in Vegetation Canopies".

Quantifying PAR

The radiometric quantity for measuring the amount of radiation falling on unit area of a surface (e.g., plant leaf) is irradiance, also known as radiant flux density. The SI (International System of Units) unit for irradiance is watts per square meter (W m^{-2}): thus, electromagnetic radiation is described in terms of the energy it carries. Generally, the term "irradiance" is used to denote the energy carried by photons regardless of their wavelength. When dealing with photons in the PAR waveband, the term "PAR irradiance" should be used to denote the irradiance contributed by photons with wavelengths between 400 and 700 nm:

$$I_{\mathrm{PAR}} = \int_{400}^{700} I_{\lambda}(\lambda)\mathrm{d}\lambda, \qquad (1)$$

where I_{λ} is spectral irradiance.

PAR measurement in plant sciences has aimed at quantitatively describing radiation as the driving force behind photosynthesis. The intensity of photosynthesis is better predicted by the number of absorbed photons than by the radiant energy received by a leaf [2, 6]. This is illustrated by the flatter, more rectangular shape of the quantum yield curve in Fig. 1 compared with that of the action spectrum. For this reason, PAR is often measured as a flux of photons, the quanta of electromagnetic radiation. As we are dealing with the PAR waveband, the particle flux is most commonly termed "photosynthetic photon flux density" or PPFD. Mathematically, PPFD is defined as the number of photons with wavelengths in the PAR waveband crossing a small surface element in unit time divided by the area of the element.

There is no official SI unit for photon flux or PPFD. A unit defined after the famous physicist, Einstein, is used to designate one mole or Avogadro's number ($N_A = 6.022 \times 10^{23}$) of photons. To describe the PPFD under natural illumination conditions, a suitable unit is thus μE m^{-2} s^{-1} (microeinsteins per square meter per second). In modern practice, however, μmol m^{-2} s^{-1} (micromoles of photons per square meter per second) is the most extensively used unit for PPFD. The increased popularity of micromoles compared with microeinsteins is explained by the common requirement of scientific publishers to use SI units whenever possible. The base unit for amount of substance of the international system of units is the mole. Although the (micro) einstein is based on the mole, it is not on the list of SI-derived units. At the same time, μmol m^{-2} s^{-1} is a combination of SI units and thus explicitly compatible with it. Use of μmol m^{-2} s^{-1} for

measuring PAR is also suggested by the International Commission on Illumination [5].

For a monochromatic beam of radiation, the flux of photons is proportional to the flux of energy. The coefficient of proportionality results from Planck law: the energy of a photon is related to its wavelength λ as $E = hc/\lambda$, where h is the Planck constant (6.34×10^{-34} J s) and c is the speed of light in vacuum ($c = 3.00 \times 10^{8}$ m s^{-1}). Thus, we may write the mathematical definition of PPFD as

$$Q_{\mathrm{PAR}} = \int_{400}^{700} \frac{I_\lambda(\lambda)}{hcN_A} \lambda \, \mathrm{d}\lambda \tag{2}$$

and define the broadband conversion factor

$$\frac{Q_{\mathrm{PAR}}}{I_{\mathrm{PAR}}} = \frac{1}{hcN_{\mathrm{A}}} \frac{\int_{400}^{700} I_\lambda(\lambda)\lambda \, \mathrm{d}\lambda}{\int_{400}^{700} I_\lambda(\lambda) \mathrm{d}\lambda}. \tag{3}$$

For a waveband such as that of PAR containing many wavelengths, the conversion factor $Q_{\mathrm{PAR}}/I_{\mathrm{PAR}}$ depends on the actual spectral composition of radiation, that is, on irradiance conditions [11]. The technical aspects of the problem are further discussed in section "Calibration and Spectral Corrections", and experimental values for PPFD to irradiance conversion are given in section "PAR Below the Atmosphere".

There have been several attempts to define PAR in the history of photosynthesis research. Currently, there is very little ambiguity in the term PAR with regard to the wavelength interval. However, other intervals have also been used [12–14], most notably the interval between 380 and 710 nm (e.g., in the Soviet Union, [15]). Thus, historical PAR measurement data may not be compatible with modern data sets despite similar measurement units: careful evaluation and recalibration is required when dealing with long time series.

PAR waveband coincides almost exactly with the visible part of the solar spectrum. The similarity of the wavelength ranges of PAR and visible light may be useful in solving scientific problems. For example, the directional distribution of diffuse sky brightness has been parametrized for different sky conditions [16] and using the high correlation between PAR and visible light, these distributions may be useful in modeling directional distribution of incident PAR. Similarly, an expression such as "availability of light" is reasonable in everyday use. In scientific literature, however, the less ambiguous term "radiation" should always be preferred to "light." Ambiguity may emerge as the science of visible light, photometry, has long traditions in quantitative measurements: a standardized luminosity function is used to describe the brightness of radiation as perceived by the human eye. The luminosity function is analogous to the action spectrum of PAR in defining the response of a biological system (the average human eye) to incident radiation. Photometric units have a strong user base with a wide field of applications. The modern unit for measuring visible light incident on a surface (illuminance), lux, was widely used in photosynthesis research half a century ago. However, despite the similarity of the luminosity function and the action spectrum, human vision is not related to the photobiology of photosynthesis, and the use of photometric units and terminology in treatment of PAR is strongly discouraged.

Fundamentals of Radiation Transfer Theory

The physical laws and concepts used in describing the complex interactions of electromagnetic waves with matter can be readily applied to describe the processes related to PAR. However, trying to follow this path would ultimately lead to tracking every wave or particle using quantum electrodynamics. While accurate laws are used, for example, to describe the scattering of radiation (including PAR) by molecules, aerosols, and cloud particles in the atmosphere, it is impractical to apply the fundamental theory to plants, vegetation canopies, or the whole planet. The common formulation used for accurate computations of PAR, called the radiative transfer theory (RTT), is a simplification based on ray optics: radiation is described in terms of photon bundles traveling in straight lines with infinite velocity.

In principle, RTT is a mathematical formulation of the law of conservation of radiative energy. Using given sources of radiation and the absorptive, scattering, and emissive properties of the medium, it predicts the detailed angular and spatial distribution of radiation. RTT describes radiation in terms of the energy it carries. However, since it is defined for monochromatic radiation, the particle and energy flows are proportional. RTT is a special case of the more general transfer theory dealing with particles (e.g., neutrons or

electrons) in a scattering, absorbing, and generating medium.

Radiative transfer theory is exactly applicable to monochromatic radiation (i.e., radiation consisting of a single wavelength). Solutions for the entire PAR waveband may be obtained by dividing the waveband into narrow spectral intervals, solving the radiative transfer equation for each wavelength, and then adding the contributions of the wavelength intervals. Thus, RTT deals with spectral radiance as the most detailed descriptor of the radiation field. (Spectral) radiance $R(\vec{\Omega})$, sometimes erroneously termed radiation intensity, is defined as the radiative energy arriving from a given direction crossing a small (imaginary) surface element per unit solid angle per unit surface area. The SI unit of radiance is W m^{-2} sr^{-1} (Watts per square meter per steradian). Evidently, $R(\vec{\Omega})$ is a function of the direction $\vec{\Omega}$, and thus describes the angular distribution of the radiation field. When dealing with the spectral characteristics of radiation, spectral radiance, or radiance per unit wavelength interval, is used. Similarly, when describing PAR, the PAR radiance $R_{\mathrm{PAR}}(\vec{\Omega})$ is used, or radiance carried by photons with wavelengths in the PAR waveband. The mathematical formulation of the theory does not depend on the wavelength interval and is the same for $R(\vec{\Omega})$ and $R_{\mathrm{PAR}}(\vec{\Omega})$. Similarly, the units of PAR radiance are those of the radiance $R(\vec{\Omega})$.

Integrating radiance over the hemisphere (corresponding to a solid angle of 2π) using cosine as the weighing function yields irradiance:

$$I\left(\vec{\Omega}\right) = \int_{2\pi} R\left(\vec{\Omega}'\right) \cos\left(\widehat{\vec{\Omega}', \vec{\Omega}}\right) \mathrm{d}\Omega', \tag{4}$$

where $\widehat{\vec{\Omega}', \vec{\Omega}}$ is the angle between the directions $\vec{\Omega}$ and $\vec{\Omega}'$. Irradiance I equals the amount of radiative energy carried through a unit area of the surface. A similar equation may be written to relate the PAR radiance R_{PAR} and the PAR irradiance I_{PAR}. From Eq. 4, it is evident that the irradiance I_{PAR} is a function of a directional variable $\vec{\Omega}$ describing the normal of the surface: for any given surface, the amount of radiative energy it receives depends on its orientation. Commonly, irradiance is measured on a horizontal surface. When measuring downward-directed flux arriving from the upper hemisphere (i.e., incident flux), $\vec{\Omega}$ points downward; when measuring reflected radiation, $\vec{\Omega}$ points upward.

Radiation flux, or the amount of radiation crossing a surface in unit time, is calculated by dividing the surface into small surface elements, finding the flux density (i.e., irradiance) for each element, and finally adding the contributions of the surface elements. In mathematical terms, the summation is performed as an integration. In this way, a quantitative measure of radiation flow can be obtained through any (possibly imaginary) surface regardless of its shape and orientation. When measuring PAR flux for estimating photosynthesis (in either quantum or energy units), the surface should be that of a plant leaf. To find PPFD on an arbitrarily inclined leaf surface, the angular distribution of the radiation field quantified by the radiance $R_{\mathrm{PAR}}(\vec{\Omega})$ has to be known. However, it is impractical, if not impossible, to measure the angular variation of radiance for each point inside a complex vegetation canopy. Under natural conditions, PAR arrives from the upper hemisphere only and to estimate the energy received, intercepted, and absorbed by a canopy, it is sufficient to measure fluxes on horizontal surfaces. This is in good accordance with the common practice of using the terms "irradiance" or "PPFD": unless specified otherwise, fluxes are measured using a horizontal (and leveled) sensor. However, for the sake of clarity, it is advisable to always specify the directionality of the radiation receiving surface when describing flux measurements.

Techniques for Measuring PAR

Sensors Used for PAR Measurements

The actual sensors used to measure PAR vary in construction and the principle behind the radiation-to-voltage conversion. Two broad classes may be defined, corresponding roughly to instruments for measuring the two quantities defined in the previous section, PPFD and PAR irradiance. Accordingly, two ideal PAR sensors may be defined: the ideal PAR quantum sensor, designed to measure PPFD, and the ideal PAR energy sensor, to measure PAR irradiance. The definition of an ideal sensor is not based on its construction quality or working principle, but on its spectral response function $\varepsilon(\lambda)$. This function, similar to the

photosynthetic action spectrum, describes the output of the instrument when illuminated by a monochromatic radiation source with wavelength λ. To obtain the response of the sensor to any natural radiation source, the spectral response function has to be integrated over the spectral sensor's sensitivity range:

$$M_{\mathrm{PAR}} = \int_{\lambda_{\min}}^{\lambda_{\max}} \varepsilon(\lambda) I_{\lambda}(\lambda) \mathrm{d}\lambda, \tag{5}$$

where M_{PAR} is the sensor reading, $\lambda_{\min}$ and $\lambda_{\max}$ define the spectral interval where the sensitivity function is nonzero, and I_{λ} is the spectral irradiance. The sensor reading M_{PAR} is usually obtained in electric units: voltage or current produced by the sensor. While M_{PAR} is not directly usable for characterization of the radiation field, it is assumed to be proportional to the radiometric quantity of interest. The coefficient of proportionality, or calibration coefficient, is discussed in the next section.

The spectral sensitivity function for an ideal PAR energy sensor is constant with wavelength, $\varepsilon_I(\lambda) = \mathrm{const}$ inside the PAR waveband. The ideal PAR quantum sensor measures the number of incident photons independent of their wavelengths. To achieve this, Planck's law prescribes that the spectral sensitivity function of an ideal PAR quantum sensor has to be proportional to wavelength, $\varepsilon_Q(\lambda) \sim \lambda$, in the spectral interval of 400–700 nm. Outside the PAR waveband, $\varepsilon_Q \equiv \varepsilon_I \equiv 0$. The spectral sensitivity functions of the two ideal sensors are presented in Fig. 2 together with the response functions of two commercially available sensors.

Real PAR quantum sensors are usually photovoltaic sensors based on the photoelectric effect. Use of the photoelectric effect makes the response to the number of photons, regardless of their wavelengths, almost linear. This also makes PAR quantum sensors very responsive: they respond to changes in PPFD almost instantly and the upper limit on temporal sampling frequency is determined by the timescale of natural PAR changes, not the technical capabilities of the sensor.

Common photovoltaic sensors are, in principle, photodiodes working in photo-galvanic regime. A complete hemispheric field of view is achieved by placing a diffuser, a carefully shaped piece of diffusely transparent material, in front of the receiving element (the diode). The spectrally nonselective nature of the diffuser material in the PAR waveband makes the receiving surface look white. A suitable filter blocks out wavelengths outside the PAR region. Choice of the filter, along with the physical design of the instrument, brings the spectral response curve closer to that of an ideal sensor. The most widely used quantum sensor is the LI-190SA by LI-COR, Inc. [17, 18] which consists of a silicon photodiode covered by a visible band-pass interference filter and a colored glass filter. Since its introduction, use of quantum sensors to measure PAR has been expanding rapidly [19–24]. Currently, PAR sensors with silicon photodiodes are manufactured by several companies (e.g., PARLite by Kipp and Zonen, E90 Quantum sensor of Jauntering International Corp, SAT-LANTIC PAR sensor for underwater measurements) and form the most commonly used PAR sensor class.

Recently, GaAsP photodiodes have become available for use in PAR sensors (e.g., QSP-2100 by

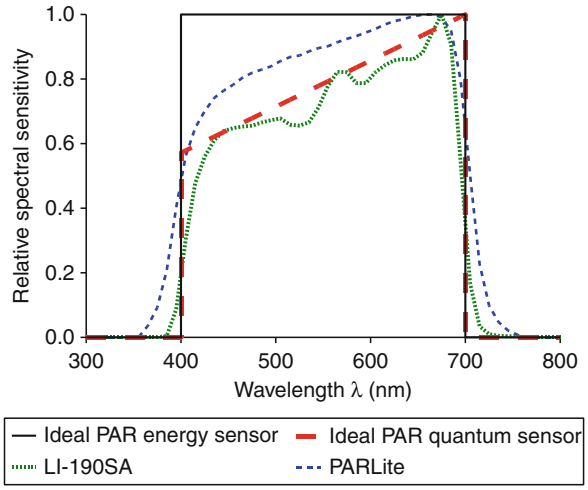

Photosynthetically Active Radiation: Measurement and Modeling. Figure 2
The relative spectral sensitivity functions (normalized so that the maximum value of each curve equals unity) of two ideal sensors for measuring PAR irradiance (Ideal PAR energy sensor) and PPFD (Ideal PAR quantum sensor) together with the curves for two real sensors (LI-COR LI-190SA and Kipp and Zonen PARLite)

Biospherical Instruments Inc., JYP 1000 by SDEC France). These sensors are inexpensive because the spectral sensitivity curve of a GaAsP photodiode is close to that of an ideal PAR quantum sensor. Wavelengths below 400 nm may be cut off by choosing a suitable material for the diffuser (usually polyacrylite), and special correction filters are not needed [25].

The second broad class of PAR sensors, PAR energy sensors, includes mostly thermoelectric instruments. These instruments are designed to measure PAR irradiance with a constant sensitivity function using a black receiving surface which is heated by incident radiation. Using a calibration coefficient, the temperature reading of the receiving surface is converted into irradiance. The receiving surface is covered by a glass filter to block photons with wavelengths outside the PAR waveband. Compared with quantum sensors, thermoelectric instruments are technically more complicated and expensive. However, such instruments can be constructed with the same bodies as standard shortwave solar radiation measurement devices, pyranometers and pyrheliometers, making the measurements robust and repeatable. The first hemispheric measurements of global, diffuse, and reflected PAR were made using pyranometers covered with hemispherical glass filters [14, 26–33] and measurements of direct solar PAR with pyrheliometers covered with flat glass filters [34–36]. A thermoelectric device for measuring submarine PAR was also constructed from a thermopile coated with Parsons' black lacquer and covered by a glass filter [37]. Compared to quantum receivers, thermoelectric instruments exhibit large inertia: changes in the temperature of the receiving surface follow the changes in irradiance after a substantial time delay. The time constant (the time it takes for the output signal to decrease by $e \simeq 2.72$ times after incident radiation is completely blocked) of common thermoelectric instruments is about 10 s. Although such timescales are reasonable when measuring incident PAR in the open (affected mainly by solar elevation and atmospheric transmission), variations in radiation fluxes inside a plant canopy happen on much shorter timescales.

An interesting novel idea is to use light emitting diodes (LEDs) in photo-galvanic regime as radiation sensors. A combination of blue and red LEDs provides an acceptable approximation of the PAR spectral curve. An inexpensive sensor consisting of blue SiC and red GaP or AlGaAs LEDs exhibited good correlation with the LI-COR LI-190SA quantum sensor when measuring global PAR [38].

The most complete way to describe radiation in the PAR waveband is to measure its spectral composition. Unfortunately, the instruments for spectral radiation measurements, spectroradiometers (more commonly called just spectrometers), have been expensive and not well suited for field measurement or long-time automatic monitoring. In recent years, developments in affordable photodiode array technology have made the construction of spectroradiometers with few or no moving parts possible. These lightweight field instruments typically measure radiation between 350 and 1,050 nm with a sampling interval of a few nanometers. However, judging from the relatively small number of published results, the simplicity, robustness, and low price of quantum sensors outweigh the increased amount of data and the higher price tag produced by a spectroradiometer. In many common applications in agriculture, horticulture, or monitoring of photosynthetic productivity, monitoring of the amount of available PAR, rather than its spectral composition, is sufficient. Nevertheless, advances in technology indicate that in the decades to come, radiometry will be shifting from broadband sensors toward spectral instruments.

Most sensors described above are intended to measure global PAR: they have been designed to integrate the radiation arriving from all directions in a hemisphere and output radiation flux density. Such sensors are also called cosine receivers after the weighing function used in the mathematical formulation of the integration formula (Eq. 4). Thus, the field of view (FOV) of a cosine receiver is 2π, the solid angle corresponding to a hemisphere. Sometimes, the FOV of an instrument is restricted to receive photons coming from a single direction, for example, the sun. Alternatively, to measure only diffuse sky radiation, sensors may be equipped with a shadow band blocking the diurnal path of the sun in the sky, or a tracking shade disc (i.e., a small disc mounted on an arm activated by a mechanical device used to keep scientific instruments directed toward the sun). To measure the direct solar

component of PAR, that is, the flux density of PAR not scattered by the atmosphere, a pyrheliometer may be equipped with glass filters; alternatively, a common hemispheric PAR sensor may be fitted with a view-limiting tube analogous to that of a pyrheliometer [39]. Unfortunately, no PAR quantum sensors specially designed to measure direct radiation are commercially available. A narrow FOV is also used to study the directional properties of radiation field: directional reflectance or directional distribution of incident radiation [40, 41]. Additionally, instruments to measure radiation arriving from all directions (corresponding to a solid angle of 4π) have been designed. Such instruments measure a quantity called radiation fluence rate and they are more commonly used in aquatic environments (see section "Description of PAR in Water").

To quantify the enormous variability of the radiation field inside and below a plant canopy, single sensors do not suffice. Elaborate systems can be combined with consumer equipment to obtain the best results. The measurement systems used in plant canopies are briefly discussed in section "Instruments for Measuring fAPAR". Although only a few of these devices include the PAR sensors described above, the implicit physical principles of radiometry in these instruments, and thus also the inherent limitations and potential errors, are exactly the same.

Calibration and Spectral Corrections

Direct comparison of two PAR sensors is not a simple task. The reading of a PAR sensor can be predicted from the reading of another sensor if the spectral sensitivity functions of both sensors are known as well as the spectral composition of incident radiation. Although most producers of PAR sensors provide the spectral response functions for their instruments, the spectral composition of incident radiation is generally unknown: the relatively stable spectral composition of extraterrestrial solar PAR is heavily altered when passing through the atmosphere. Inside a plant canopy, the spectral composition of PAR is further distorted by the removal of photons at blue and red wavelengths, where the absorptance of plant leaves is the highest. Thus, care must be taken when comparing the numerical outputs of different sensors in radiation absorption measurements as well as during calibration.

To calibrate a PAR sensor, one needs to measure its output in a controlled experimental situation (e.g., using a calibration lamp) where the value of the measured quantity is known. A calibration coefficient is the ratio of the actual value of the measurable quantity (e.g., I_{PAR}) to the instrument reading (M_{PAR}):

$$\mu_I = \frac{I_{\mathrm{PAR}}}{M_{\mathrm{PAR}}} = \frac{\int_{400}^{700} I_{\lambda,\mathrm{LAMP}}(\lambda)\mathrm{d}\lambda}{\int_{\lambda_{\min}}^{\lambda_{\max}} \varepsilon(\lambda) I_{\lambda\,\mathrm{LAMP}}(\lambda)\mathrm{d}\lambda}. \tag{6}$$

Two calibration coefficients are usually provided for PAR sensors: one to convert the sensor's reading into energy units (W m^{-2}) defined by Eq. 6 and one for quantum units (μmol m^{-2} s^{-1}). The coefficient for quantum units is defined similarly to that for energy units, $\mu_Q = Q_{\mathrm{PAR}}/M_{\mathrm{PAR}}$.

Most manufacturers calibrate the sensors in laboratory using standard lamps, which is indicated by using the subscript LAMP for the spectral irradiance in Eq. 6, $I_{\lambda,\mathrm{LAMP}}$. Thus, the manufacturers can control (within a given measurement uncertainty of a few percent determined by the calibration of the lamp) both the energy content and the spectral composition of incident radiation. If the spectral sensitivity of the actual sensor being calibrated deviates from that of the perfect sensor, as it invariably does, the calibration coefficient depends on the spectral composition of incident radiation. Therefore, the laboratory-derived calibration is only directly valid for irradiation by a calibration lamp and does not hold exactly under field conditions.

The errors arising from the mismatch of the predicted and actual field conditions are usually called spectral errors. Spectral errors depend on the spectral sensitivity of the sensor, the spectral composition of incident irradiance, and the spectral composition of radiation used to calibrate the sensor. Mathematically, the spectral error in PAR irradiance measurements can be written as

$$\beta_I = \frac{\mu_I \int_{\lambda_{\min}}^{\lambda_{\max}} \varepsilon(\lambda) I_\lambda(\lambda)\mathrm{d}\lambda}{\int_{400}^{700} I_\lambda(\lambda)\mathrm{d}\lambda}. \tag{7}$$

After substituting the expression for μ_I from Eq. 6 into Eq. 7, it becomes clear that spectral errors

disappear if (1) the sensor has a response function identical to that of the ideal sensor, $\varepsilon(\lambda) \equiv \varepsilon_I(\lambda)$, or (2) the irradiance conditions match the calibration lamp spectrum, $I_\lambda(\lambda) \equiv I_{\lambda,\mathrm{LAMP}}(\lambda)$ in the spectral interval from $\lambda_{\min}$ to $\lambda_{\max}$. The magnitude of the actual spectral error varies with sensor type. While it is reasonably small for the LI-190SA sensor, usually less than 1% for natural irradiance conditions, many other sensor exhibit considerably larger errors, especially under artificial illumination [11].

If the spectral composition of incident radiation or, more specifically, the difference between the spectral composition of radiation occurring during field measurements and during calibration, spectral error can be eliminated by using a spectral correction. It is evident that in the presence of the spectral error, multiplying the measurement result by the inverse of β_I (Eq. 7) would compensate completely for the differences in the spectra of incident radiation. Thus, if the actual spectral irradiance $I_\lambda(\lambda)$ is known, a spectral correction can be easily calculated. However, since $I_\lambda(\lambda)$ is usually not available, a general value characterizing the illumination conditions (clear or cloudy sky, different artificial light sources), $I_{\lambda,\mathrm{EST}}(\lambda)$, is used instead. Thus, the spectral correction factor is calculated as the reciprocal of β_I after replacing $I_\lambda(\lambda)$ by $I_{\lambda,\mathrm{EST}}(\lambda)$ in Eq. 7.

Therefore, when taking a measurement, the instrument reading is first multiplied by the calibration coefficient (μ_I or μ_Q, calculated individually for each sensor) and, optionally, by a spectral correction (calculated for a whole instrument class or model). As only the average spectral irradiance distribution for typical conditions is known, it is often preferable to ignore spectral corrections.

Another possibility to calibrate the sensors is to compare them with a reference sensor (or a spectroradiometer) with a reliable calibration by the manufacturer. When performing calibration under irradiance conditions reasonably close to those occurring under true measurement situations, spectral corrections are not required. For example, field calibrations of radiation measuring instruments are standard for the Baseline Surface Radiation Network (BSRN, [42]), an international network for global measurements of solar and atmospheric radiation at the highest available accuracy. Additionally, all PAR sensors continuously exposed to outdoor conditions should be checked regularly against well-maintained reference instruments. The sensitivity of sensors is apt to change due the aging of the diffuser and filters. Such aging is usually also documented in the instrument manual. When a frequently and reliably calibrated instrument is not available, it is strongly recommended to have a reference instrument stored under controlled conditions for periodical comparisons with the operating sensors.

Measurement Errors

As with all measurements, errors are inevitable and arise from (1) the impossibility of controlling all the physical processes that determine the measurement result, (2) the non-perfect construction of the measuring apparatus, and (3) the spectral composition of incident radiation. Since the last error source (spectral errors) was covered in section "Calibration and Spectral Corrections", only the first two categories are briefly discussed here.

Measurement errors can be reduced by carefully following the instructions for performing the measurements (usually provided by the manufacturer), using proper installment and maintenance procedures (e.g., checking for the directionality and leveling of the instrument), checking the performance of the instrument regularly, and accounting for material degradation and changes in operating environment (ambient temperature, irradiance conditions, humidity, etc.). Flux measurements with a hemispherically integrating sensor suffer from directionality effects: the sensor is not equally sensitive to radiation arriving from different directions. While manufacturing imperfections or physical damage may cause an instrument to have random sensitivity fluctuations with the azimuth angle of an incident beam, sensitivity to polar angle (or zenith angle for a leveled sensor looking upward) of the radiation source is usually more systematic. The dependence of sensitivity with the polar angle is called the cosine response of the sensor and the corresponding correction a cosine correction. The cosine response characteristics of several sensors designed for irradiance measurements, including two LI-COR 190 PAR sensors, are given in [43]. Cosine effects, together with leveling inaccuracies, are especially influential when a strong directional radiation

source is present, such as the direct solar radiation beam on a clear day. All these errors, some systematic and some random, can add to the spectral errors affecting instruments designed for measuring radiation in a spectral waveband as discussed in the previous section.

The official relative uncertainty of PAR instruments claimed by manufacturers, about 5%, can only be achieved under optimal conditions. During routine measurements, even if performed by trained specialists, the uncertainty can be considerably larger. For example, [44] gives an estimate of 10% uncertainty for PAR measurements in the FLUXNET network; a comparison performed by BSRN found significant systematic differences between different PAR sensor models and up to 20% spread within the group of 11 tested LI-190SA sensors [45].

PAR in Various Environments

PAR Below the Atmosphere

Without the influence of the atmosphere, the PAR irradiance would be determined by the solar spectrum and geometric conditions like the slightly varying distance from the earth to the sun, local solar elevation, and topographic shadowing. The spectral composition of radiation would be constant to the accuracy of the multiple scattering contribution of non-flat topography (illuminated slopes of mountains and valleys). Such direct topographic effects, although significant in shadow areas, are usually small when direct solar radiation is present and will be ignored hereafter. Under natural conditions, the amount and spectral composition of radiation in the PAR spectral band, in addition to the distance from the sun to the earth and solar elevation angle, is mainly determined by the presence of clouds, the amount and optical properties of aerosols, and, to a lesser extent, the chemical composition of the atmosphere.

Due to its universal nature, radiative transfer theory (RTT, section "Fundamentals of Radiation Transfer Theory") can be (and also has been) applied to predict the irradiation conditions under all possible atmospheric conditions. The actual precision of prediction is limited by the availability of input data and computer power. Models based on RTT can be used to calculate accurately the spectral irradiance for the different wavelengths comprising PAR, with subsequent integration to obtain I_{PAR}. For many practical purposes, however, simpler models applicable to longer timescales (hours, days, growing seasons) are sought and thus different broad-band models or physically based parametrizations are often used. For clear skies, the accuracy of the best broadband models is comparable to that of routine irradiance measurements in existing networks [46].

Models developed for predicting the behavior of sunlight in the atmosphere deal not only with PAR but with the whole shortwave spectral region. The shortwave spectral region is loosely defined as the range of wavelengths containing the bulk of the solar spectrum (magnitude wise), usually between 300 and 4,000 nm. The simplest case, global shortwave irradiance under a cloudless atmosphere, can be very accurately predicted when the following parameters are known (REST2 model, [46]): solar zenith angle, Ångström turbidity coefficient (i.e., aerosol optical depth at 1,000 nm), Ångström wavelength exponents, aerosol single-scattering albedo, air pressure, amounts of precipitable water and ozone, and ground albedo. These parameters allow to calculate the irradiance in two separate wavebands, PAR and short-wave infrared. To predict only PAR irradiance, a few parameters less are required, since ozone and water vapor have little influence on PAR.

Because not all of the listed atmospheric parameters are readily available, models based on easily measurable radiation field characteristics have also been developed [24, 47, 48]. Usually, parametrizations are based on approximately four parameters. While one parameter is always solar elevation, others describe the state of the atmosphere and can be either obtained from radiation measurements (e.g., ratio of diffuse to direct shortwave irradiance) [49] or routine meteorological data (e.g., dew point temperature). The variables explaining the majority of variance in PAR availability and the spectral quality of PAR (Q_{PAR}/I_{PAR} ratio) include solar elevation and a parameter to describe the turbidity of the atmosphere (e.g., a sky clearness parameter or the Ångström turbidity coefficient) [39, 47, 48, 50, 51].

Two downwelling PAR field components can be distinguished under a clear sky: the quasi-parallel direct beam arriving from the direction of the sun (with PAR irradiance on a horizontal surface $I_{PAR,dir}$) and the diffuse sky radiation arriving from all upward directions not blocked by topography ($I_{PAR,diff}$).

The sum of the two components is called global PAR, $I_{PAR} = I_{PAR,dir} + I_{PAR,diff}$. Depending on aerosol load and solar elevation, the ratio of diffuse PAR to global PAR irradiance on a horizontal surface ranges between 20% and 40% [52]. The presence of clouds decreases the global PAR irradiance usually by up to 80% [41] and the contribution of diffuse PAR irradiance may take any value between that corresponding to a clear sky and 100%. If the cloud cover is broken, the existence of the direct beam depends on the locations of gaps between clouds. Thus, two temporally and spatially variable phenomena have great influence on the amount of diffuse PAR: aerosol loading and clouds. Although the effect of aerosols may be dominating in places with low average cloud cover, it is expected that the contribution of clouds as the source of variations in diffuse PAR is larger for most locations.

The fraction of PAR in global shortwave irradiation I_{PAR}/I_{SW} varies little and is usually between 40% and 50% [53, 54]; values above 50% occur under very low sun, thick cloud cover, or rain [14]. As an example, measurements at Tõravere actinometric station (Estonia) are presented in Fig. 3 for variable cloud conditions during June 2009. The global PAR irradiance can be relatively reliably predicted from global shortwave irradiance, $I_{PAR} = 0.43\ I_{SW}$. The contribution of diffuse PAR irradiance $I_{PAR,diff}$ to global shortwave irradiance, on the other hand, was more variable (Fig. 3). Under completely overcast skies, the diffuse PAR irradiance $I_{PAR,diff}$ equals the global PAR irradiance I_{PAR}, which, as usual, contributed about 43% of global shortwave irradiance. Under clear skies, $I_{PAR,diff}$ is significantly smaller than I_{PAR}: in Fig. 3 the data points corresponding to clear sky form the lower cluster. Broken cloud cover conditions are represented by $I_{PAR,diff}$ values between the two extremes when plotted against I_{SW}.

Some variation in I_{PAR}/I_{SW} with elevation above sea level is expected, but this variation is difficult to detect [52]. However, using measurement sites at 550, 900, and 1,500 m above sea level, an increasing trend was noted with altitude, of 3.6% per km for hourly values of Q_{PAR}/I_{SW} under clear skies [55]. An inverse trend was found for hourly Q_{PAR}/I_{SW} under cloudy weather conditions: Q_{PAR}/I_{SW} decreased at a rate of 1.8% per km.

The spectral composition of global PAR is relatively stable [56]. It is reflected in the near-constant value of

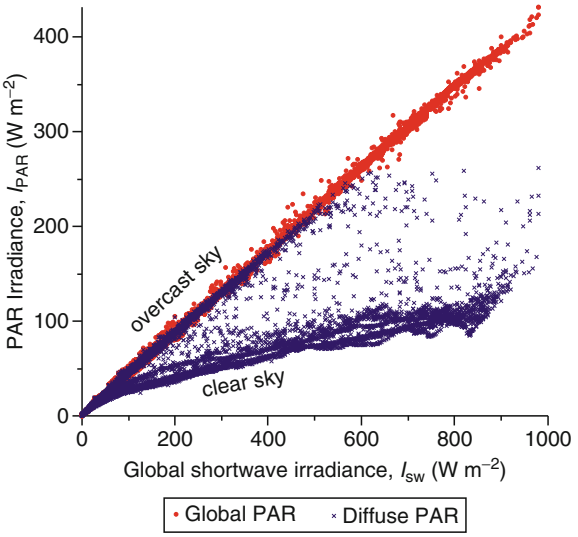

Photosynthetically Active Radiation: Measurement and Modeling. Figure 3
Global and diffuse PAR irradiance as functions of global shortwave irradiance in Tõravere, Estonia, in June 2009. Sky condition varied from clear to completely overcast. The labels "clear sky" and "overcast sky" indicate the characteristic values of diffuse PAR irradiance for the two atmospheric conditions

the ratio of PPFD to PAR irradiance, Q_{PAR}/I_{PAR} (Eq. 3). The classical value of $Q_{PAR}/I_{PAR} = 4.57$ μmol s^{-1} W^{-1} for global PAR proposed by McCree [2] has been verified by several later studies. For example, [57] reported that while 1-min average of Q_{PAR}/I_{PAR} varied from 4.23 to 4.68 μmol s^{-1} W^{-1}, 1-h averages were relatively insensitive to atmospheric composition with $Q_{PAR}/I_{PAR} = 4.56$ μmol s^{-1} W^{-1} for global PAR.

For the diffuse radiation field component, the ratio depends on atmospheric conditions. Under a blue sky, an average value of $Q_{PAR,diff}/I_{PAR,diff} = 4.28$ μmol s^{-1} W^{-1} was reported [52] along with the observation that the ratio increases with aerosol load. In the presence of clouds, $Q_{PAR,diff}/I_{PAR,diff}$ increases with increasing cloud cover from 4.24 μmol s^{-1} W^{-1} (a value characteristic of blue sky) to the constant value for global radiation, $Q_{PAR}/I_{PAR} = 4.57$ μmol s^{-1} W^{-1} under an overcast sky [57]. The value of Q_{PAR}/I_{PAR} (or $Q_{PAR,diff}/I_{PAR,diff}$) describes the color of light: the smaller the ratio, the bluer the light looks to the human eye.

The angular distribution of PAR radiance can be approximated using models applicable to visible

light [16]. Additionally, several approximations exist for predicting the angular distribution of shortwave radiation. These models have been parametrized for use in the PAR waveband [40, 41] for different atmospheric conditions ranging from completely clear to overcast sky. The angular models describe sky radiance relative to the nadir direction and cannot be generally used to describe global PAR irradiance or PPFD.

A final remark on the spectral quality of PAR at the bottom of the atmosphere can be made based on the spectral composition of extraterrestrial solar radiation. The I_{PAR}/I_{SW} ratio outside the atmosphere based on the solar constant of $I_{SW} = 1367\ W\ m^{-2}$ equals 38.8% [51]. Using $Q_{PAR} = 2426\ \mu mol\ s^{-1}\ m^{-2}$ for the extraterrestrial irradiance on a surface perpendicular to sunrays [48], we obtain that the Q_{PAR}/I_{PAR} ratio outside the atmosphere equals 4.57 $\mu mol\ s^{-1}\ W^{-1}$ – exactly that proposed by McCree [2]. While it may be concluded that the atmosphere has little effect on the spectral quality of PAR, the exact coincidence is most likely due to chance: an accuracy of two decimals is clearly beyond the uncertainties inherent in radiation measurements.

Description of PAR in Water

The waveband of radiation allowing phytoplankton to carry out photosynthesis (i.e., PAR) corresponds approximately to the same spectral band of electromagnetic radiation that penetrates into water. Pure water absorbs strongly in the ultraviolet ($\lambda < 400$ nm) and near-infrared ($\lambda > 700$ nm) spectral regions [58]. Otherwise, the underwater light field is determined by the incident irradiance (see section "PAR Below the Atmosphere"), the state and composition of the water body, and the optical properties of its bottom.

The spectrum of solar radiation penetrating a water body changes drastically as its irradiance diminishes with depth. While the scattering of radiation is commonly rather insensitive to wavelength in the PAR waveband, absorption by different components has a very strong spectral effect. The components having an optical effect are dissolved organic substances (also known as yellow substance), different species of phytoplankton, and inert particulate matter (Fig. 4). Since the concentration of these is highly variable, the spectral distribution of underwater irradiance in the PAR waveband can change rapidly.

In a vertically homogeneous water body, the value of the downwelling spectral irradiance I_λ diminishes approximately exponentially with depth z, that is, Beer's law holds (see also Eq. 8):

$$I_\lambda(z) = I_\lambda(0) \exp\left[-\int_0^z K_{diff}(\lambda, z')\mathrm{d}z'\right]$$

where $K_{diff}(\lambda,z)$ is the diffuse attenuation coefficient, a parameter often used to describe the optical properties of natural water bodies [62–64].

In addition to the spectral PAR irradiance I_λ and PPFD, a quantity called spectral fluence rate, or spectral spherical irradiance, is sometimes used to describe the amount of radiation in water. It is defined as the total amount of photons incident in unit time interval from all directions on a small sphere, divided by the

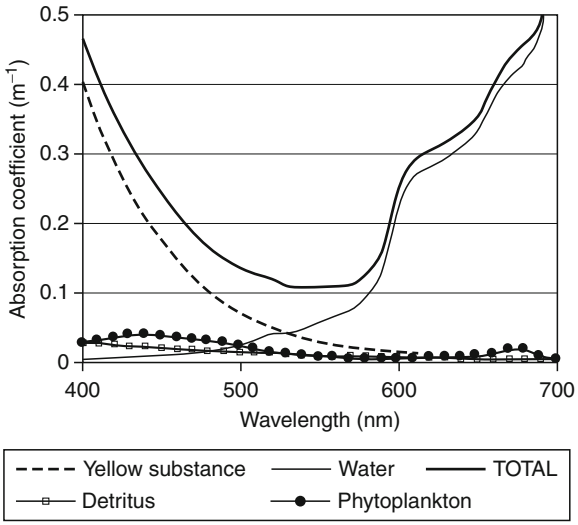

Photosynthetically Active Radiation: Measurement and Modeling. Figure 4
Decomposing the absorption spectrum of a water sample. Spectra of the absorption coefficients corresponding to pure fresh water [59]; 1.0×10^{-3} mg m^{-3} yellow substance (specific absorption coefficient at 380 nm 0.565 L mg^{-1} nm^{-1}); 1.0 mg m^{-3} chlorophyll-a (phytoplankton, [60]); and detritus (from the measured data of [61]). The total absorption of the water sample is plotted with a bold line

cross-sectional area of the sphere. Analogously to the PAR irradiance I_{PAR}, the PAR fluence rate may be defined by integrating over the PAR waveband. As both fluence rate and irradiance describe the amount of PAR in water, Beer's law can (with a different attenuation coefficient) also be applied to describe the change in spectral fluence rate with depth.

Beer's law is valid only for the spectral irradiance $I(\lambda)$, that is, the irradiance in a narrow spectral interval around wavelength λ. Many authors have shown that the exponential law fails when a single value of K_{diff} is applied over the whole PAR waveband. The reason for this failure lies in the change of spectral composition of PAR with depth. This can be illustrated using the wavelength corresponding to maximum penetration, λ^*, and the Q_{PAR}/I_{PAR} ratio. In clear oceanic waters, λ^* corresponds to the maximum in the extraterrestrial solar spectrum (~460 nm). When increasing the amount of optically active substances in water, λ^* is shifted toward larger values, as shown in Table 1, and can be even larger than 700 nm in brownish boreal lakes [65].

Photosynthesis in water takes place mainly in the so-called euphotic layer near the surface. At the bottom of the euphotic layer, the downward PAR irradiance has decreased to 1% of its value just below the surface [66]. In clear oceanic waters, the thickness of the euphotic layer can be of the order of a hundred meters. As a contrast, in turbid lakes, the layer may be only half a meter thick. Ice cover, and especially ice covered with snow, may substantially decrease the amount of PAR in water to a level not sufficient for even the minimum amount of photosynthetic activity, thus creating anoxic conditions [67].

Similarly to other environments, the PAR irradiance in water can be given in energy units (I_{PAR}, W m^{-2}) or quantum units (Q_{PAR}, µmol s^{-1} m^{-2}). The quanta-to-energy ratio Q_{PAR}/I_{PAR} (µmol s^{-1} W^{-1}) changes with the variation of the spectral distribution of irradiance. Above water, Q_{PAR}/I_{PAR} is practically constant with an average value Q_{PAR}/I_{PAR} = 4.57 µmol s^{-1} W^{-1} over a wide range of conditions (see section "PAR Below the Atmosphere"). In clear oceanic water, Q_{PAR}/I_{PAR} decreases with depth. As a contrast, in turbid coastal waters and lakes, it increases with depth and approaches an asymptotic value. Thus, sufficiently deep below the surface of turbid waters, the spectral distribution of PAR, but not the value of PAR irradiance, can be considered almost constant. The average value of Q_{PAR}/I_{PAR} there has been estimated at 4.15 ± 0.40 µmol s^{-1} W^{-1} [68]; a value of Q_{PAR}/I_{PAR} = 4.45 ± 0.48 µmol s^{-1} W^{-1} has been suggested for Norwegian coastal waters [69]. In lakes, Q_{PAR}/I_{PAR} varies from 4.72 to 5.86 µmol s^{-1} W^{-1} [65]. Additionally, there is a strong linear correlation between Q_{PAR}/I_{PAR} and K_{diff} (r = 0.95) and, in deeper waters, Q_{PAR}/I_{PAR} can be estimated using K_{diff} measurements in the surface layer [65].

Measurement Stations and Networks

Unfortunately, no international network to measuring PAR currently exists. As can be seen from their documentation, large international radiation measurement networks like the Baseline Surface Radiation Network (BSRN http://www.gewex.org/bsrn.html) [70] have discussed the subject of PAR measurements, but standardized measurements have not started. The PAR irradiance (and also APAR) is recorded as a by-product in some networks specialized in other measurements. For example, the FLUXNET project (http://daac.ornl.gov/FLUXNET/) [71, 72], which is aimed at

Photosynthetically Active Radiation: Measurement and Modeling. Table 1 Wavelength of maximum penetration λ^*, ratio Q_{PAR}/I_{PAR}, and relative difference D of Q_{PAR}/I_{PAR} from its value above the surface for different water types as classified by [62]

Water type	I	II	III	1	3	5	7	9
λ^* (nm)	465	480	505	530	540	547	565	582
Q_{PAR}/I_{PAR} (µmol s^{-1} W^{-1})	3.9	4.0	4.2	4.4	4.5	4.5	4.7	4.9
D (%)	16	14	9	4	2	2	2	6

quantifying the exchanges of carbon dioxide, water vapor, and energy between the biosphere and atmosphere, has PAR data available for many sites. The solar radiation budget network SURFRAD (http://www.srrb.noaa.gov/surfrad/) [73] measures, among other variables, the incident PAR irradiance. A promising start is SolRad-Net (http://solrad-net.gsfc.nasa.gov/), a companion to the successful global AERONET aerosol network. However, the number of SolRad-Net sites where PAR is measured today is still very small. Routine monitoring of PAR and APAR as key factors in global photosynthetic productivity [74] has been proposed several times. Currently, the only global data sets available are those based on remote sensing data (see section "APAR and fAPAR from Satellite Observations"). Although remote sensing can provide excellent spatial coverage unachievable in any ground-based network, indirect remote retrievals should still be validated against direct measurements of the variable under investigation.

PAR in Vegetation Canopies

PAR Absorption by Leaves

PAR Absorption by Leaf Pigments Electromagnetic radiation in the PAR spectral domain is mainly absorbed by photosynthetic pigments in the leaf. Among these, chlorophylls a and b are the most important. They are found across a wide range of species, from algae to higher plants, and they participate in transforming radiation into energy, which is later stored as chemical bonds of carbohydrates. Chlorophylls are characterized by two absorption peaks at 450 and 670 nm corresponding to the blue and red color, respectively, explaining the green color of leaves (Fig. 5). Besides chlorophylls, green leaves contain also other pigments. Pigments such as carotenes and xanthophylls belonging to the carotenoid family associated with chlorophylls are known to improve radiation harvesting. They mainly absorb in the blue region with absorption peaks at 450 and 470 nm making them look orange or yellow. Additionally, carotenoids prevent oxidation of the photosynthetic system in case of excess incident radiation. Other pigments like anthocyans absorb radiation in the PAR waveband with maximum absorption between 450 and 600 nm [77]. They protect the leaf against UV radiation by preventing formation of free radicals and are responsible for the reddish colors of some leaves during the autumn. The rest of the biochemical leaf constituents responsible for the brown color (such as polyphenols, which develop during leaf senescence), although absorbing in the PAR waveband (Fig. 5), have no direct role in photosynthetic processes.

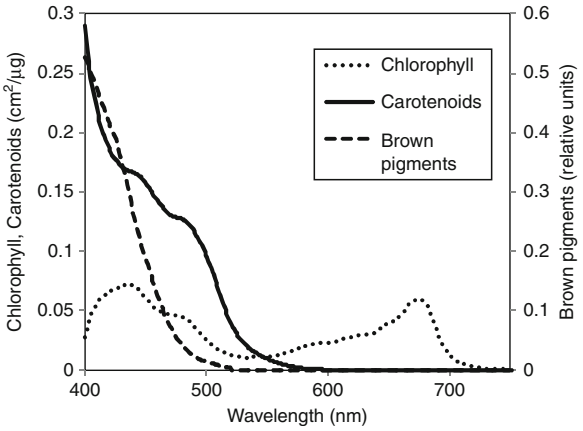

Photosynthetically Active Radiation: Measurement and Modeling. Figure 5
Specific absorption coefficients of chlorophyll (a + b), carotenoids and brown pigments from the PROSPECT model [75, 76]

The Role of Leaf Structure The efficiency with which a leaf absorbs visible radiation depends not only on chlorophyll content per unit leaf area, but also on the specific mechanisms plants have developed to utilize radiation. Chlorophylls are concentrated in chloroplasts, mainly located in the palisade mesophyll consisting of tightly packed elongated cells just under the upper epidermis (Fig. 6). The tubular shape of palisade cells enhances the forward propagation of PAR, thus directing photons to the chloroplasts located at the bottom of the palisade. In a number of species, the epidermis cells act as lens focusing radiation on the chloroplasts thus increasing radiation absorption by the photosynthetic pigments [78]. The spongy mesophyll of higher plants contains little PAR-absorbing pigments. Instead, the numerous voids in this layer act as a mirror to scatter back a large fraction of the radiation transmitted through the palisade mesophyll, further improving absorption of radiation by chloroplasts.

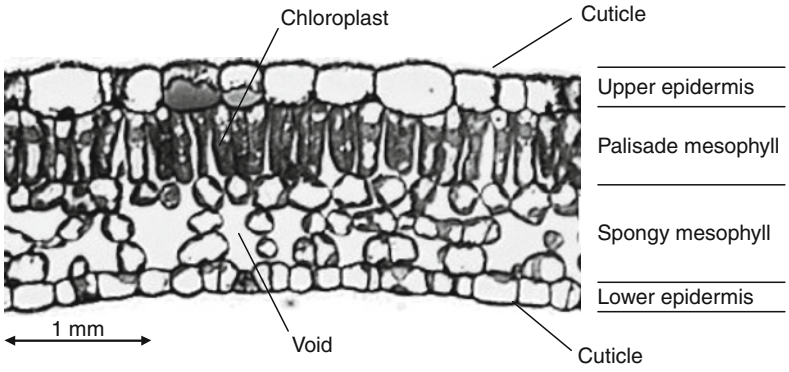

Photosynthetically Active Radiation: Measurement and Modeling. Figure 6
Structure of a typical dicotyledon leaf (young maple)

When the capacity of the leaf to use the available PAR is exhausted by drought or nutrient stress, plants may use different strategies to minimize absorbed radiation. Besides changing the orientation of a leaf away from direct sunlight, adaptations have been developed at the upper epidermis level. The cuticle may turn to crystalline and the amount of hair on the leaf surface may increase, thus also increasing the leaf reflectivity and directing radiation away from chloroplasts.

The Fate of Absorbed PAR in the Leaf The energy carried by photons absorbed by the leaf is transformed into several types of energy. The dominant type is heat, accounting for more than 75% of the absorbed PAR energy. Therefore, only a maximum of 25% of APAR is left for photosynthesis. When photosynthesis is limited by temperature, water, or nutrient availability, the radiation use efficiency of a leaf decreases even further. Additionally, a part of the excess PAR energy absorbed by the pigments may be dissipated as fluorescence, that is, reradiated as photons with different, longer wavelengths.

Under optimal water, temperature, and nutrient conditions, the efficiency of photosynthesis at the leaf level is determined both by the absorbed PPFD and the CO_2 concentration in the leaf [79]. Figure 7 shows that the photosynthetic rate increases almost linearly with incident PPFD up to some threshold value. After the threshold is reached, the rate of photosynthesis becomes constant, limited by the CO_2 concentration in the leaf. This concentration in the leaf, in turn, is driven by the CO_2 concentration in the atmosphere

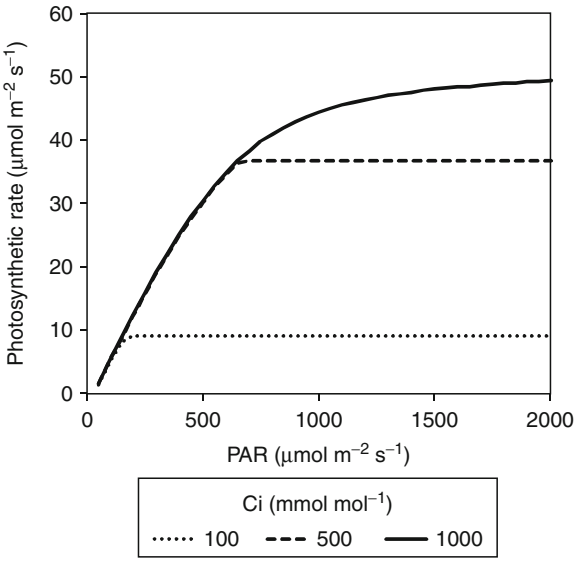

Photosynthetically Active Radiation: Measurement and Modeling. Figure 7
Relation between incident PAR photon flux density and photosynthesis rate at different intercellular concentration of CO_2 (C_i), simulated using model of C3 photosynthesis [79]

and the stomatal conductance of the leaf, itself determined by the hydraulic status of the leaf and the plant as a whole [80]. The maximum photosynthetic rate, achieved at large PPFD values, also strongly depends on the fraction of the incident PAR absorbed by the leaf [81], which is determined mostly by leaf chlorophyll content.

Since chlorophyll absorbs the majority of incident PAR and uses only a small fraction of it for photosynthesis, the excess energy must be dissipated in a way that keeps the photosynthetic apparatus functional. For this purpose, plants have developed several photoprotection mechanisms. One of such mechanisms is based on xanthophyll pigments: the conversion of violaxanthin into zeaxanthin can remove the excess energy from chlorophyll and dissipate it as heat. When conditions become more favorable, this conversion is reversed, and zeaxanthin is changed back to violaxanthin. The status of the xanthophyll cycle may be used to evaluate the various stresses experienced by plants, since it affects the leaf optical properties, or leaf reflectance spectrum, in the 500–600 nm spectral region [82].

The second pathway for dissipating excess energy absorbed by photosynthetic pigments is fluorescence. When photosynthesis is limited by stress factors or when a leaf is exposed to too high irradiance, a small but measurable fraction of the excess energy is reemitted at a longer wavelength than that of absorption. The peak of chlorophyll fluorescence emission is in the blue-green (455 nm), red (685 nm), and far-red (735 nm) spectral regions [83]. The energy lost in this process amounts to a few percent of the total PAR energy absorbed by the leaf [84].

Quantitative Description of PAR in Vegetation Canopies

Radiative Transfer in Plant Canopies When dealing with PAR in vegetation canopies [85, 86], it is assumed that the only scatterers are plant leaves (or needles, shoots, etc.), that radiation originates from the sun only, and that thermal emission can be ignored. Thermal emission in the PAR waveband is indeed negligible (nonexistent for all practical purposes) at temperatures suitable for photosynthesis. The existence of fluorescence by green leaves, an emission source concurrent with photosynthesis, assumes the presence of incident PAR. The energy contribution of fluorescence is small compared to that of scattered PAR, and is generally masked by scattered radiation [87].

When using RTT, the optical thickness of a canopy is often described by its leaf area index (LAI): one-sided leaf area (or half of the total leaf area for plants with non-flat leaves) per unit ground area. Quite commonly, the downward cumulative LAI, $L(z)$, calculated as LAI above height z, is used instead of the geometric vertical coordinate z. At the top of the canopy, $L(z_{\text{top}})$ equals 0, then increases with depth inside the canopy. Finally, below the plant layer, $L(0) = \text{LAI}$.

Radiation Interception When RTT is applied to describe the attenuation of radiation in vegetation, a well-known result is obtained. In an environment where the scattering elements fill a volume uniformly and randomly, and are infinitesimally small, the radiance decreases exponentially:

$$R_{\text{PAR}} = R_{\text{PAR}}\left(z_{\text{top}}\right) e^{-kx}, \tag{8}$$

where $R_{PAR}(z_{top})$ is the radiance before entering the scattering medium, k is the attenuation coefficient, and x is the distance from the point where radiation enters the medium (depth inside the canopy). The exponential decay described by Eq. 8 is commonly known as Beer's law, sometimes called Beer–Lambert's or Beer–Lambert–Bouguer's law. The terms attenuation and interception are used interchangeably: interception of radiation attenuates the unscattered radiation field.

The tradition of using Beer law for radiation transmission in vegetation canopies consisting of flat leaves started with the classic work by Monsi and Saeki [88, 89]. They plotted the logarithms of light transmittance of vegetation canopies during overcast days against the LAI of the canopy, and obtained straight lines (Fig. 8). They explained the variations in the slopes of the lines (i.e., attenuation coefficients) theoretically, using leaf inclination angles. Since then, Beer's law has been routinely applied to approximate PAR availability in plant canopies [90, 91].

Generally, Beer's law is exactly valid for monochromatic radiation only and is not directly applicable to radiation arriving from the whole hemisphere (i.e., irradiance I_{PAR}). To obtain non-intercepted PAR irradiance on a horizontal surface below a plant canopy, Beer's law (Eq. 8) has to be integrated over the upper hemisphere:

$$I_{\text{PAR}} = \int_0^{\pi/2} \int_0^{2\pi} R_{\text{PAR}}(z_{\text{top}}, \vartheta, \phi) \mathrm{e}^{-k(\vartheta,\phi)x(\vartheta,\phi)} \times \cos\vartheta \sin\vartheta \, \mathrm{d}\theta \mathrm{d}\phi, \tag{9}$$

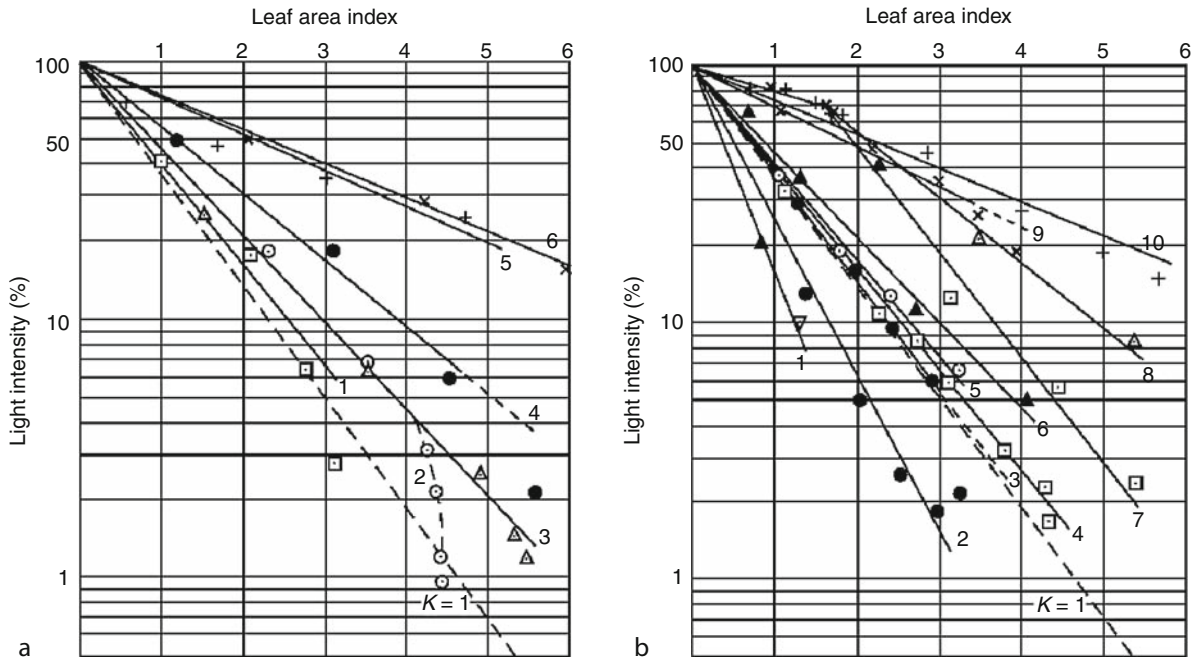

Photosynthetically Active Radiation: Measurement and Modeling. Figure 8
Light intensity–leaf area index curves of some plant communities measured under mostly overcast conditions on different days (Reprinted from [89]). (**a**) The communities of the Kirigamine montane meadow; (**b**) the communities of the Tazima meadow and in the vicinity of Tokyo. Light intensity, a good proxy for PAR irradiance, decreases near-exponentially (See the original article for more details. Published with permission from Oxford University Press)

where ϑ and ϕ are the zenith and azimuth coordinates describing a direction in the upper hemisphere, respectively. The distance from the bottom to the top of the canopy in the direction (ϑ,ϕ) depends mostly on the zenith angle ϑ. For a canopy layer of uniform thickness, $x(\vartheta,\phi) = 1/\cos\vartheta$. Equation 9 is identical to the equation relating irradiance and radiance, Eq. 4. The former can be obtained from the latter by expressing radiance as a function of canopy transmittance (which is Beer's law for vegetation canopies, Eq. 8) and considering that the differential of a solid angle can be expressed in polar coordinates as $d\Omega = \sin\vartheta\, d\theta d\phi$. Computations involving numerical integrations of canopy interceptance over the upper hemisphere similar to Eq. 9 are common in optical estimations of LAI [92, 93].

In most applications of RTT, the probability of a scattering event, and thus the extinction coefficient k, does not depend on the direction (ϑ,ϕ) of photon travel. However, this does not generally hold in a vegetation canopy of flat leaves. For example, in a canopy consisting of mainly horizontal leaves, the probability of hitting a leaf is much larger for a photon traveling in the vertical direction than for one traveling in the horizontal direction. Thus, the Ross–Nilson G-function (a function returning a value between zero and one for every direction) is used to describe the effect of foliage orientation: it equals the ratio of leaf area projected in a given direction (ϑ,ϕ) to the total leaf area [85].

The distribution of foliage inside a natural canopy is not uniform and the assumptions of Beer's law are not fulfilled. To accurately describe the attenuation of radiation (including PAR) inside vegetation, more complex methods have to be used, and one must take into account the structure of the vegetation layer. In addition to the above-mentioned angular distribution of foliage, additional variables describing the geometric properties of plants at various levels (shoot, branch, crown, etc.) have to be used. Introduction of larger-scale structures decreases interception at the top of the canopy and increases it in middle canopy layers [94, 95].

Scattering Inside the Canopy The small fraction of photons in the PAR waveband not absorbed when hitting a leaf give rise to a phenomenon commonly known as beam enrichment. After one or two scatterings in the canopy (very few photons in the PAR waveband survive more), photons may be inserted back into the beam traveling in the direction of the receiver. In other words, as plant leaves are not black (completely absorbing), the downward flux of radiation is "enriched" by scattered photons. Naturally, the amplitude of this effect depends on the scattering properties of the scattering elements, leaves, and needles.

To describe the reflectance and transmittance properties of plant leaves, they are usually assumed to be Lambertian surfaces – the angular distribution of reflected (or transmitted) radiance does not depend on the direction of scattering. Actual leaves deviate from Lambertian surfaces, mainly due to the specular (mirror-like) reflectance from the wax coating. However, for practical purposes, there is no information that the assumption of Lambertian scattering would lead to considerable errors [96]. Therefore, the scattering properties of flat leaves are generally described by up to three numbers: the two leaf reflectance values for the abaxial and adaxial leaf sides, and one leaf transmittance (the general reciprocity relations require for the two sides of a Lambertian surface to have identical transmittance [95]). However, quite often reflectances are not available separately for the two leaf sides and the reflectances of the adaxial and abaxial sides are taken equal.

The reflectance properties of leaves depend somewhat on species, growing conditions, and leaf status. Some approximate values are given in the literature. In his seminal book, Ross used the values 0.06 and 0.09 for leaf reflectance and transmittance in the PAR region, respectively [85]. Relatively little between-species variability in leaf optical properties, compared to within-species variability, was found during an extensive study in Texas, USA [97], indicating that the leaf optical properties in this spectral region are dynamically stable along a pronounced climate gradient. For trees and shrubs, a leaf reflectance of 0.09 (standard deviation 0.01) and a leaf transmittance of 0.06 ($\pm$0.03) was proposed; for grasses the resulting numbers were 0.12 ($\pm$0.01) for reflectance and 0.06 ($\pm$0.02) for transmittance [97]. Although the measurements were performed in the spectral interval of channel 1 of the AVHRR satellite sensor (550–700 nm) which corresponds to the green–red part of PAR, they can also be used to approximate the leaf optical properties in the whole PAR waveband with reasonably small errors.

Radiation Field Inside a Vegetation Canopy Canopy photosynthesis depends not only on the amount of available PAR, but also on how the irradiance is distributed: high and low PAR irradiance levels have different photosynthetic potentials. Without going into further details, it is possible to divide the locations inside a plant canopy into three groups.

1. Full sunlight. In areas inside the canopy where the sun is completely visible, or "sunflecks," the radiation field is strongly dominated by the direct solar radiation beam. Under natural conditions, one can safely ignore the contribution of scattered PAR and assume that the spectral distribution of radiation is identical to that above the canopy.
2. Penumbra. Due to the nonzero diameter of the solar disc, shadows cast by sunrays do not have sharp edges. Full sunlight and complete shadow are always separated by a narrow strip with smoothly varying irradiance. If the angular dimensions of the shadowing object are smaller than the apparent diameter of the solar disc, for example, the object is far from the receiver, no complete shadowing can occur. Depending on the fraction of the solar disc visible, the PAR flux and spectrum in penumbra may be close to what they would be under either direct sunlight or complete shadow.
3. Shadow (umbra). Behind large objects or sufficiently deep down into the canopy, the direct solar irradiance can be considered zero. Thus, the radiation conditions in umbra are determined by the possible presence of diffuse sky radiation, radiation scattered by plant elements, and radiation reflected by the underlying soil. The spectral composition of radiation depends on skylight conditions, the amount of visible sky, and the spectral properties of canopy elements. On an overcast day, the whole canopy is effectively in a shadow cast by clouds.

The division as given above is just one of the possible approaches to categorizing the radiation field. No standard practice has emerged yet in the scientific literature: the word "sunfleck" is the general term used to

describe areas with increased irradiance, whereas the penumbra is often ignored. Depending on application, the penumbra may be treated as either an area where the sun is obstructed (i.e., shadow) or, in contrast, an area where the irradiance is above the threshold determined by the reading below a dense canopy (i.e., sunfleck).

Due to the dynamic nature of sunflecks, the radiation field inside a canopy can be highly variable, both spatially and temporally [98]. Variations in the diffuse field are generally much smaller, and thus global irradiance in umbra is much easier to measure. For this reason, canopy transmittance measurements made on a cloudy day are much more representative. For example, 412 radiometers would be required to estimate the instantaneous downward radiation flux in a pine stand with a maximum error of 10% in the midday flux above the canopy, whereas just one instrument is needed for a full-day average in a hardwood canopy [99]. When averaged over the path, the sun follows on a day or a growing season, the mean transmittance of direct radiation can be approximated by a single measurement of transmittance of diffuse sky radiation. However, due to natural limitations in the solar elevation and azimuth angles which are specific to each geographic location, systematic errors may occur [90].

Even if one has sufficient data to quantify the average PAR irradiance inside and below a vegetation canopy, this will not suffice for photosynthesis modeling purposes. It has been known for a long time that the photosynthetic response of a leaf is not linear with PAR irradiance (see section "PAR in Vegetation Canopies"). Thus, the radiation field is commonly described as composed of two fluxes, direct and diffuse PAR, and PPFD values at leaf surfaces are calculated separately for the two fluxes [100]. Beside atmospheric conditions, the availability of direct solar radiation depends only on canopy structure. In contrast, diffuse radiation is generated via more numerous mechanisms.

The first source of what can be called diffuse radiation, or radiation of diminished radiance compared with direct solar radiance above the vegetation canopy, is penumbra. Penumbral effects are purely geometric and are most evident in a tall canopy of small scatterers, for example, in a needle-leaf boreal forest. At high latitudes, low sun angles further increase the pathlength of direct solar beam in the canopy, thus making the penumbra dominate the radiation field on a clear day. In a canopy consisting of shoots, the penumbral effect alters the irradiance distribution, but also vertically redistributes the photosynthetic potential inside the canopy [101]. Coupling the nonzero angular diameter of the sun and the three-dimensional structure of the vegetation canopy can lead (at least in model calculations) to an increase in canopy photosynthetic capacity by tens of percent [102, 103]. Such computations are rare in the scientific literature since the correct prediction of penumbral irradiation assumes nonzero scatterer sizes, which is beyond the scope of traditional RTT.

The second source of diffuse radiation, multiple scattering inside vegetation, depends on the canopy structure and cannot be easily predicted without a radiative transfer model. However, whereas modeling penumbra requires special consideration for both the spatial distribution and the dimensions of canopy elements, the dimensions of leaves are usually ignored when calculating multiple scattered radiation fluxes. Assuming infinitesimally small leaves makes it possible to apply the traditional methods for solving RTT [85, 86].

The third component of the diffuse PAR field inside a vegetation canopy is contributed by diffuse sky radiation: some of the photons scattered by the atmosphere can penetrate the vegetation layer without being intercepted by canopy elements. Depending on cloudiness and other atmospheric conditions, the diffuse sky irradiance can vary within large limits. The complications related to calculating this PAR component originate in the difficulties of correctly estimating the variability of above-canopy diffuse radiance. In contrast, the canopy transmittance can be modeled from simple structural assumptions or measured from hemispheric photography.

The diffuse sky PAR irradiance is usually less than one-third of the global PAR irradiance (section "PAR Below the Atmosphere"). Considering that not all of the sky is visible inside the canopy, the diffuse PAR irradiance (on a horizontal surface) is at least one order of magnitude smaller than the direct PAR irradiance in a sunfleck. The adaptation of leaves in deeper canopy layers (where sunflecks are rare) to low irradiances makes diffuse sky radiation more effective in inducing photosynthesis than direct PAR [104]. In other words, the light use efficiency is generally larger

for diffuse radiation than for direct irradiance: this effect is sometimes termed diffuse-radiation fertilization. Thus, an increase in diffuse PAR can lead to increased carbon assimilation. This mechanism has been proposed as the explanation of the decrease in global CO_2 concentration after Mt. Pinatubo's eruption in 1991. Volcanic eruptions are known to increase the amount of atmospheric aerosol for several years thus enhancing diffuse sky radiation [105, 106] and global carbon assimilation. The adverse effect of decreasing the amount of anthropogenic sulfate aerosol could similarly lead to a decrease or fall in global photosynthesis [107].

The spectral distribution of PAR above and below a vegetation canopy is shown in Fig. 9. Four spectral distributions are shown, corresponding to global and diffuse radiation above and below a closed alder canopy (LAI = 2). The distributions are normalized so that their maximum value in the PAR waveband equals unity. Whereas changes in the spectral distribution of global PAR are relatively small, alteration of the spectral distribution for the diffuse field is quite significant. Above the canopy, the diffuse radiation spectrum peaks at blue wavelengths. The diffuse PAR field below a canopy reaches its maximum at about 550 nm, which corresponds to green light. Further, in the near-infrared (NIR) region, at wavelengths immediately above 700 nm, the diffuse spectral irradiance below the canopy increases to levels much higher than those in the PAR waveband. Such an increase emphasizes the requirement to consider spectral errors with care: if the sensor sensitivity cutoff at 700 nm is not sharp enough, measurements of diffuse PAR inside a vegetation canopy are contaminated by the high NIR irradiance. Also, the differing spectral composition of diffuse radiation between the higher and lower canopy layers must be taken into account when calculating the contribution of diffuse radiation to canopy photosynthesis.

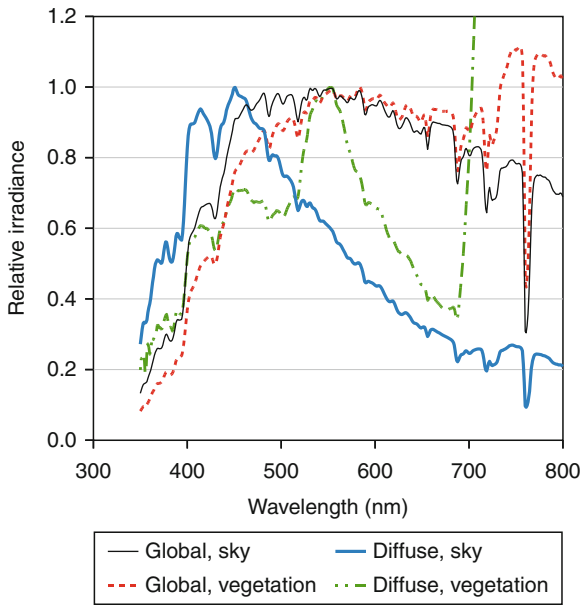

Photosynthetically Active Radiation: Measurement and Modeling. Figure 9
Spectral distribution of radiation on a clear day above and below a vegetation canopy. Measurements were made inside and next to a gray alder (*Alnus incana*) plantation (leaf area index L = 2.1) in Tõravere, Estonia

Explicit treatment of the total PAR available for photosynthesis is thus a complex task [98]. Exact computations require that many factors are taken into account: dimensions of the solar disc and the scattering elements, detailed structure of the vegetation canopy, spectral properties of leaves, nongreen canopy elements and soil, spectral and angular distributions of incident radiation, etc. Due to the large spatial and temporal variability of PAR inside a plant canopy, its measurement and empirical analysis are also extremely complicated and only a few examples are presented in the literature [20, 108].

Measurement of PAR Absorbed by Canopies

Direct Measurement of APAR The PAR flux absorbed by plant canopies (APAR) may be either measured directly using PAR sensors or estimated indirectly, based on canopy gap fraction measurements. Leaf area index (LAI) measurements may also be used to estimate the PAR absorbed by the canopy. First, a description of direct PAR measurements is given.

The PAR absorbed by vegetation equals the total amount of radiative energy absorbed by all plant surfaces and can thus be measured in either quantum or energy units. The formulation of the problem is identical for the two representations. Here, the quantum APAR (Q^4_{PAR}) is used as an example. Due to the different spectral compositions of PAR that is incident or reflected and transmitted by a vegetation canopy,

converting between Q^A_{PAR} and its companion quantity in energy units, I^A_{PAR}, is not a straightforward task. Thus, estimates of fAPAR from quantum measurements are not directly comparable with fAPAR values calculated in energy units. However, considering the measurement uncertainties and the errors related to retrieval of fAPAR from remote sensing measurements, the differences are ignored here.

Q^A_{PAR} is computed from the energy conservation law in the canopy using hemispherical fluxes:

$$Q^A_{\mathrm{PAR}} = Q^{\downarrow}_{\mathrm{PAR}}(z_{\mathrm{top}}) - Q^{\uparrow}_{\mathrm{PAR}}(z_{\mathrm{top}}) - Q^{\downarrow}_{\mathrm{PAR}}(0) + Q^{\uparrow}_{\mathrm{PAR}}(0). \quad (10)$$

where $Q^{*}_{\mathrm{PAR}}(z)$ represents downward $Q^{\downarrow}_{\mathrm{PAR}}(z)$ or upward $Q^{\uparrow}_{\mathrm{PAR}}(z)$ hemispherical PAR fluxes at the bottom ($z = 0$) or top ($z = z_{top}$) of the canopy. Therefore, the hemispherical PAR sensors should be precisely located to obtain representative measurements of the several terms in the PAR balance:

- $Q^{\downarrow}_{\mathrm{PAR}}(z_{\mathrm{top}})$, the incident PAR at the top of the canopy is measured using upward-looking sensors at the top of the canopy
- $Q^{\uparrow}_{\mathrm{PAR}}(z_{\mathrm{top}})$, the reflected PAR is measured using downward-looking sensors at the top of the canopy
- $Q^{\downarrow}_{\mathrm{PAR}}(0)$, the transmitted PAR is measured by upward-looking sensors placed at the bottom of the canopy
- $Q^{\uparrow}_{\mathrm{PAR}}(0)$, the PAR reflected by the soil is measured using downward-looking sensors at the bottom of the canopy

The number of sensors used to measure the several terms in a representative way depends mainly on the heterogeneity of the canopy and on the typical footprint of the sensor. About half of the flux collected by a hemispherical sensor comes from inside a circle whose radius equals the distance of the sensor from the object it is looking at [109]; about 96% of the signal originates from inside a circle with a radius of five times the distance. Therefore, many sensors (between 5 and 50) are required to properly measure all the terms in Eq. 10 at the bottom of the canopy: the distance from the sensor to the bottom of the canopy (when measuring $Q^{\downarrow}_{\mathrm{PAR}}(0)$) or the soil (when measuring $Q^{\uparrow}_{\mathrm{PAR}}(0)$) is generally limited. Conversely, just one sensor is required for the incoming PAR, $Q^{\downarrow}_{\mathrm{PAR}}(z_{\mathrm{top}})$, and only a few for the reflected PAR, $Q^{\uparrow}_{\mathrm{PAR}}(z_{\mathrm{top}})$, depending on the distance between the sensor and the top of the canopy (Fig. 10).

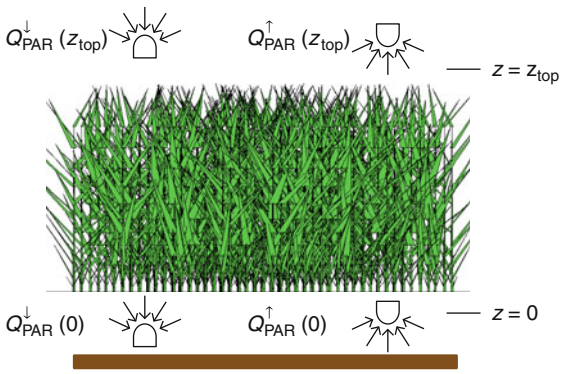

Photosynthetically Active Radiation: Measurement and Modeling. Figure 10
Configuration of PAR sensors to measure APAR and fAPAR. Sensor A measures the incident PAR $\left(Q^{\downarrow}_{\mathrm{PAR}}(z_{\mathrm{top}})\right)$, sensor B measures the reflected PAR $\left(Q^{\uparrow}_{\mathrm{PAR}}(z_{\mathrm{top}})\right)$, sensor C measures the transmitted PAR $\left(Q^{\downarrow}_{\mathrm{PAR}}(0)\right)$, and sensor D (usually omitted) measures the soil reflectance $\left(Q^{\uparrow}_{\mathrm{PAR}}(0)\right)$

The fraction of absorbed PAR $\left(\mathrm{fAPAR}, F^A_{\mathrm{PAR}}\right)$, may be derived from Eq. 10 by dividing all the terms by the incident PAR:

$$F^A_{\mathrm{PAR}} = 1 - r_{\mathrm{CAN}} - t_{\mathrm{CAN}}(1 - r_{\mathrm{SOIL}}), \quad (11)$$

where r_{CAN} is the reflectance of the canopy, t_{CAN} is the transmittance of the canopy, and r_{SOIL} is the soil reflectance. As mentioned above, F^A_{PAR} is used here to denote the quantum fAPAR, or the absorbed fraction of incident photons in the PAR waveband. Note that all these variables are bihemispherical quantities [110, 111], although the directional integration of incident radiation requires, as a minimum, weighing the direct and diffuse components of canopy transmittance. According to Eq. 11, fAPAR is a very convenient quantity: it is independent on the magnitude of the incident irradiance. However, fAPAR is somewhat sensitive to the irradiance geometry: the attenuation of the direct component of the incident radiation field varies strongly with the direction of the sun as well as canopy characteristics.

If the soil reflectance r_{SOIL} is assumed to be known, the PAR balance may be approximated by using measurement data for the three first terms only, that is, the incident $\left(Q^{\downarrow}_{PAR}(z_{top})\right)$, reflected $\left(Q^{\uparrow}_{PAR}(z_{top})\right)$, and transmitted $\left(Q^{\downarrow}_{PAR}(0)\right)$ radiation. Equation 11 may further be simplified as in the PAR domain, where very little multiple scattering is expected,

$$F^{A}_{PAR} \simeq (1 - t_{CAN})(1 - r_{\infty}), \tag{12}$$

where r_{∞} is the asymptotic value of canopy reflectance when the leaf area index, L, tends toward infinity. Values of r_{∞} are generally small in the PAR domain (around 0.06 [112]) since most photons are absorbed by the green leaves. In these conditions, the PAR balance, Eq. 10, may be approximated by measuring only the incident $\left(Q^{\downarrow}_{PAR}(z_{top})\right)$ and the transmitted $\left(Q^{\downarrow}_{PAR}(0)\right)$ terms. It is thus possible to avoid problems in measuring the soil reflectance r_{SOIL}: as highlighted earlier, many sensors are required due to the small distance between soil and sensor and the possible effect of the sensor shadow in its footprint. It also avoids problems related to the dependence of r_{SOIL} on the directionality of incident radiation.

Because the PAR balance and thus fAPAR both depend on the varying illumination geometry, continuous measurements are required. Furthermore, fAPAR measurements are generally used in light-use efficiency models [3, 113] which require daily and even seasonally integrated fAPAR values. The PAR radiance measurement system thus needs to be set in place from several days up to several months. In practice, this calls for weatherproof systems with sufficient autonomy both in terms of energy and memory. Affordable systems meeting these requirements and able to replicate individual observations for improved spatial sampling have been developed only recently. However, instantaneous measurements using several view directions may be achieved by different existing systems, allowing the reconstruction of fAPAR values for any (possibly modeled) illumination geometry.

In all situations, the approach based on radiation balance assesses the value of PAR absorbed by the canopy, independently of the nature of the radiation intercepting elements. As a consequence, when non-photosynthetic material (such as trunks, branches, or senescent leaves) constitutes a significant fraction of canopy, the true fAPAR, or PAR absorbed by the green photosynthetically active elements, is overestimated.

Estimation of fAPAR from fIPAR Green leaves generally absorb a very large fraction of light in the PAR domain, that is, they appear almost black from a pure radiative standpoint. Considering this, the fraction of absorbed PAR may be approximated by the fraction of intercepted PAR (fIPAR, F^{I}_{PAR}):

$$F^{A}_{PAR} = 1 - t_{CAN}. \tag{13}$$

Combining Eqs. 12 and 13 provides a relation between the fraction of absorbed PAR and the intercepted fraction:

$$F^{A}_{PAR} = F^{I}_{PAR}(1 - r_{\infty}).$$

The validity of this approximation has been extensively investigated and found to hold with reasonable accuracy [114–117].

Instruments for Measuring fAPAR

Directional and Flux Measurements Based on the directionality of measurements, fAPAR sensors can be divided into two subgroups. The first group contains instruments that disregard the directional distribution of incident PAR (either by integrating over the upper hemisphere or looking into only one particular direction); the second group consists of instruments measuring with a field of view divided between different directions (multidirectional devices). Generally, the lack of directional sampling by instruments in the first group must be compensated by increased spatial sampling.

Ceptometers are devices consisting of an array of hemispherical sensors aligned on a single support, allowing for spatial representativeness. They are particularly well suited for crops: a ceptometer covering a transect representative of a forest canopy would be too long to be moved easily between the measurement locations. While a ceptometer is used to measure radiation below the canopy, the incident PAR can be simultaneously recorded with an additional PAR sensor. Examples of such sensor arrays are AccuPAR (Decagon, USA), SunScan (Delta-T, UK), and PAR/LE (Solems, France).

Other specialized multipoint radiation measurement systems have been developed (for mainly in-house use) on various scales. For example, spatial distributions of the radiation field (with focus on PAR) affecting a conifer shoot have been measured using optical fibers and a CCD matrix [118]. At the other end of the scale are systems capable of characterizing tree-level heterogeneity using hundreds of sensors attached to 5-m-long booms [119]. PAR @METER [120] is a recently developed device capable of continuously monitoring the transmitted PAR at different points inside and above a vegetation canopy. Incident and transmitted PAR are simultaneously recorded and stored in a network of sensors placed according to a predefined spatial sampling scheme using wireless computer connections.

Directional devices are generally less common than the hemispherical instruments listed above. Examples of directional, below-canopy radiation measuring devices are TRAC (Natural Resources, Canada) and DEMON (CSIRO, Australia). They measure direct sunlight and use different approximations to characterize the plant architecture. TRAC inverts the light transmittance profiles obtained on a transect based on a model of canopy gap size distribution [121]. It accounts for the nonhomogeneous distribution of foliage in certain canopies (also called clumping effect [122]) by inverting the measured sunfleck length distribution. DEMON makes use of Beer's law and a special zenith angle at which canopy transmittance does not depend on leaf orientation [123] to retrieve LAI from incident and transmitted PAR measurements.

The instruments mentioned above are designed for measurements of transmitted PAR. However, by adding canopy reflectance measurements, the complete PAR balance can be obtained (Fig. 10). From such balance measurements, it is also possible to calculate the fraction of absorbed PAR, fAPAR.

Multidirectional Transmission Instruments The incoming PAR may be decomposed into the direct component coming from the sun and the diffuse component due to light scattering in the atmosphere. For each of those components, a fAPAR value can be associated. The total fAPAR can then be written as:

$$F^A_{PAR} = \left(1 - f_{diff}\right) F^A_{PAR}(\Omega_S) + f_{diff} F^A_{PAR}(2\pi^+), \quad (14)$$

where f_{diff} is the diffuse fraction of radiation in global irradiance, Ω_S is the direction of the sun, and $2\pi^+$ is used to denote the upper hemisphere; $F^A_{\text{PAR}}(\Omega_S)$ and $F^A_{\text{PAR}}(2\pi^+)$ are thus the fAPAR values for direct-only or diffuse-only incidence, respectively. Sometimes, $F^A_{\text{PAR}}(\Omega_S)$ is called the black-sky fAPAR and correspondingly, $F^A_{\text{PAR}}(2\pi^+)$ the white-sky fAPAR. To apply Eq. 14 to the calculation of F^A_{PAR} for all sky conditions, the directional characteristics of t_{CAN} (Ω) have to be known.

Directional devices provide measurements of canopy transmittance, t_{CAN} (Ω), in a number of directions $\Omega = (\vartheta,\phi)$. Two types of devices are mainly used: the LAI-2000 instrument [124] and digital hemispherical cameras (DHC) [125, 126]. Lidar systems may also access the directional variation of light transmittance, although the technique might be better suited for other applications related to detailed characterization of canopy architecture. The LAI-2000 instrument measures light transmitted in the blue wavelengths to the bottom of the canopy in five concentric rings of 15° in the range $0 < \vartheta < 70°$. For each ring, all azimuths directions are accounted for. Measurements are generally taken under diffuse conditions to prevent an unwanted sensitivity to the specific sun direction, while minimizing any possible sun glint on the leaves. The blue spectral region is used since, at these wavelengths, leaves appear almost black and diffuse sky scattering is at its peak. The view azimuth angle can be modified using a series of view-limiting caps to block out a part of the sky or focus the measurements toward specific directions of interest.

Hemispherical cameras provide estimates of the gap fraction over the whole hemisphere. If the angular distribution of incident radiation is known, the gap fraction may be converted into canopy non-interceptance. Again, assuming that leaves are black at the visible wavelengths used by cameras, the canopy interceptance is converted into canopy absorptance. DHC usually involves a high-resolution digital camera and an attached fisheye lens. This fisheye lens projects the whole upper hemisphere onto the digital array of the camera, producing circular images. However, historical data recorded on black-and-white film may still be encountered and, in some cases, photographs made using ordinary lens are used (i.e., any lens not covering the whole hemisphere). The a posteriori processing of digital images provides the fraction of the upper

hemisphere covered by vegetation. This is done by classifying each pixel as sky or non-sky, that is, applying a threshold to divide the pixels constituting the image into two classes [126].

Furthermore, the variations in vegetation canopy transmittance with zenith (and sometimes also azimuth) angle may be used to reconstruct the diurnal variation of fAPAR. Note that, similarly to sensors measuring the transmitted PAR, no distinction is made between green photosynthetically active elements and the non-photosynthetic material. This may lead to an overestimation of the actual value of the true fAPAR. However, when using hemispherical photographs taken from above canopies, it may be possible to distinguish between green and nongreen elements. Unfortunately, downward looking photography is limited to relatively short canopies for obvious practical reasons. DHC techniques are very efficient by allowing instantaneous measurements that can be replicated multiple times to improve the spatial sampling while accessing the diurnal variation of fAPAR. However, such measurements are only representative of the current canopy architecture, and measurements should be repeated along the growing season to match the canopy architecture dynamics.

A novel approach consists in using digital cameras as hemispherical radiation receivers [127, 128]. Similarly to the traditional DHC approach, a fish-eye lens projects the whole hemisphere onto the sensor array. However, instead of just applying a threshold to identify the gaps in the canopy, the new "calibrated camera" method treats the receiving surface of the camera as a two-dimensional array of miniature quantum receivers. Each array element receives radiation from a single direction in the upper hemisphere. The spectral sensitivity functions of the array elements have maxima in the optical region of electromagnetic radiation, that is, in the PAR waveband. Therefore, after proper laboratory calibration, a raw digital image stored in the camera can be treated as a (PAR) radiance measurement result. However, these measurements must be treated with care because modern consumer cameras are complex optical systems designed for producing visually good-looking images, not recording spectral radiance values.

Relationships Between fAPAR and LAI The devices described above are often used (or even designed) for measuring canopy leaf area index (LAI) [92, 93]. Generally, all techniques to estimate LAI from PAR transmittance measurements rely on Beer's law (Eq. 8). The directional instruments allow for a more accurate integration over the hemisphere required for the accurate application of Beer's law. However, a direct use of it, without spectral integration, is still quite common when relating PAR irradiance and LAI [129]. The opposite link is also often made: if the canopy LAI is known, fAPAR can be modeled using the known optical properties of the elements constituting the vegetation canopy and some basic knowledge of canopy structure. All these calculations are based on the Beer's law specially formulated for vegetation canopies, as described in section "Quantitative Description of PAR in Vegetation Canopies".

APAR and fAPAR from Satellite Observations

The fraction of absorbed photosynthetically active radiation, fAPAR was probably the first biophysical variable to be estimated from remote sensing observations from NDVI, the normalized difference vegetation index computed as $\mathrm{NDVI} = \frac{r_{\mathrm{NIR}} - r_{\mathrm{RED}}}{r_{\mathrm{NIR}} + r_{\mathrm{RED}}}$, where r_{NIR} and r_{RED} are the top-of-canopy reflectance in the near-infrared (NIR) and red (RED) bands, respectively [130]. The early empirical relationships were later explained by investigating the radiative transfer in canopies [112, 131]. Compared to other biophysical variables (such as LAI), fAPAR appears to be retrievable much more accurately and robustly [132, 133]. The optimal configuration for retrieving fAPAR includes four spectral bands: red, near-infrared, green, and red edge. Simple observations in the red and near-infrared in view directions close to nadir were found to lead to slightly degraded performance.

The optimal view angle for a satellite instrument is not directly down (nadir), but in the principal solar plane close to the hot spot (the direction of the sun, corresponding to backward scattering), and in the perpendicular solar plane at zenith angles close that of the sun [132, 133]. Alternatively, directions around 60° from nadir in the backscattering direction or in the perpendicular plane were also shown to be close to optimal [134]. However, as these optimal configurations are not generally available, most algorithms for fAPAR retrieval focus on the minimization of

directional effects by simply making use of whatever remote sensing data can be obtained.

In addition to NDVI, indices have been developed to correct for the contribution of soil to the measured reflectance, or to use the more readily available top-of-atmosphere reflectance instead of the top-of-canopy value [116, 134]. Further, look-up tables have been used to derive fAPAR from MODIS top-of-canopy reflectance observations after calibration with radiative transfer model simulations [135]. However, when the physically based algorithm (known as the main algorithm) fails, a backup algorithm is triggered using relationships between fAPAR and MODIS NDVI. Neural networks have also been used [120, 136] to operationally retrieve fAPAR from satellite-measured radiances.

The main fAPAR products derived from satellite observations (Table 2) thus demonstrate a wide range of either empirical or physically based approaches. To obtain these fAPAR products, the needed inputs are either top-of-canopy or top-of-atmosphere reflectance values observed in 2–13 reflectance bands. Some

Photosynthetically Active Radiation: Measurement and Modeling. Table 2 Examples of fAPAR values derived from satellite-based reflectance measurements

Product name	Approach	Sensor	Reference
NDVI	Empirical linear regression	AVHRR	[130, 137, 140]
NDVI	Linear regression of RT simulations	AVHRR	[112, 141]
RDVI	Linear regression of RT simulations	POLDER	[134]
JRC-FAPAR	VI calibrated using RT simulations	PARASOL, SEVIRI	[116]
TOC-VEG	NN calibrated using RT simulations	MERIS	[136]
TOA-VEG	NN calibrated using RT simulations	MERIS	[142]
MODIS	LUT from RT simulations	MODIS	[135]
CYCLOPES	NN calibrated using RT simulations	Vegetation	[120]
GLOBCARBON	Derived from LAI product	Vegetation, MERIS, AATSR	[143]
GEOLAND2	NN calibrated using other products	Vegetation	[144]

VI vegetation index, *RT* radiative transfer, *NN* neural network, *LUT* look-up table

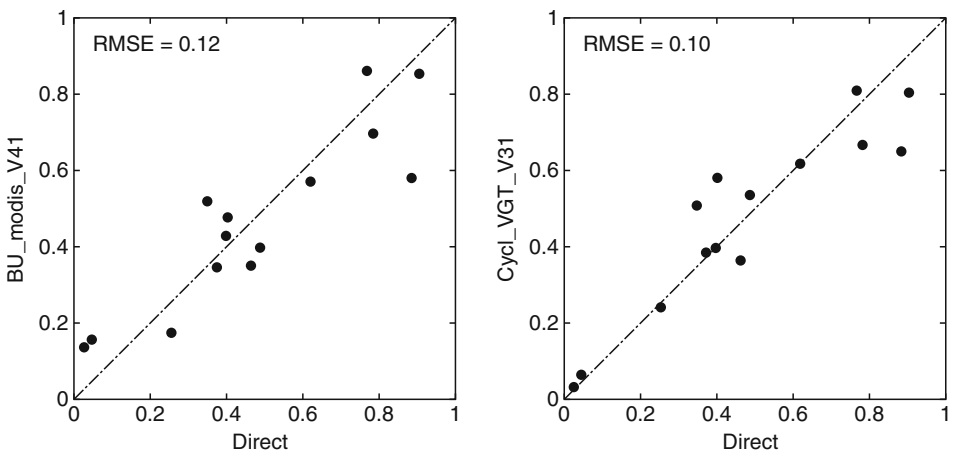

Photosynthetically Active Radiation: Measurement and Modeling. Figure 11
Comparison of ground-measured (horizontal axis) and satellite (vertical axis) estimates (MODIS: left, CYCLOPES: right) of fAPAR

algorithms use a priori information on vegetation type or rely on a land cover map. Most of the algorithms provide an instantaneous black-sky fAPAR value at the time of satellite overpass, while a few others use multidirectional observations, to provide a daily integrated black-sky value. Note that most of the polar orbiting sensors considered here are on satellites in sun-synchronous orbits with equatorial crossing time close to 10:00 local time. Under these conditions, the instantaneous black-sky fAPAR value is a good approximation of the daily integrated fAPAR value.

Individual validation exercises have been reported by several authors [116, 137–139]. They generally show a reasonable agreement between ground-measured fAPAR and satellite estimates, with RMSE values around 0.10–0.15 (in fAPAR units) (Fig. 11). Considering the complex interactions between radiation and vegetation canopies described above, fAPAR also has a most desirable feature: it is almost independent of scale. Values of fAPAR derived from algorithms applied at higher spatial resolution and integrated over a coarser spatial domain provide similar values to those derived using the same algorithm applied directly to the coarser spatial resolution [133]. Unfortunately, the same cannot be said of any other vegetation parameter derived from remote sensing data.

Future Directions

The current research related to PAR measurement (and, inevitably, modeling) is aimed at utilizing the technological advances in (remote) sensing technology to better characterize the environment we live in. Photosynthesis is the energy source for all life on earth. The raw energy for life is originally dispersed in the form of electromagnetic radiation arriving from our closest star. Although the importance of photosynthesis, and the role of shortwave radiation in it, has always been acknowledged, there are still large gaps in our understanding.

From a more technical point of view, the most evident and surprising gap is a lack of comprehensive ground-based measurement network. Fortunately, this lack of basic monitoring does not result in severe ignorance of global PAR availability. This is evidenced by the ongoing satellite measurements and the simultaneous model developments – to convert satellite sensor readings into radiation fluxes absorbed by vegetation hundreds of kilometers below. The progress is also witnessed by the large number of scientific articles with keywords such as fAPAR, satellite remote sensing, and global productivity. The ultimate goal of this research, however, is not only to give a detailed quantitative measure of the health of our planet, but also to provide the physical basis for describing and understanding the very fundamental links between the physical and biological environments.

Bibliography

1. McCree KJ (1972) The action spectrum, absorptance and quantum yield of photosynthesis in crop plants. Agric Meteorol 9(3–4):191–216
2. McCree KJ (1972) Test of current definitions of photosynthetically active radiation against leaf photosynthesis data. Agric Meteorol 10(6):443–453
3. Monteith JL (1977) Climate and efficiency of crop production in Britain. Philos Trans R Soc Lond B Biol Sci 281(980):277–294
4. Shibles R (1976) Terminology pertaining to photosynthesis. Crop Sci 16(3):437–439
5. CIE (1993) Terminology for photosynthetically active radiation for plants. CIE Collect Photobiol Photochem 106(6):42–46, ISBN 3900734461
6. McCree KJ (1965) Light measurements in plant growth investigations. Nature 206(4983):527–528
7. Inada K (1976) Action spectra for photosynthesis in higher-plants. Plant Cell Physiol 17(2):355–365
8. Barnes C, Tibbitts T, Sager J, Deitzer G, Bubenheim D, Koerner G, Bugbee B (1993) Accuracy of quantum sensors measuring yield photon flux and photosynthetic photon flux. Hortscience 28(12):1197–1200
9. Bonhomme R (2000) Beware of comparing RUE values calculated from PAR vs solar radiation or absorbed vs intercepted radiation. Field Crops Res 68(3):247–252, cited By (since 1996) 16
10. Sinclair TR, Muchow RC (1999) Radiation use efficiency. Adv Agron 65:215–265
11. Ross J, Sulev M (2000) Sources of errors in measurements of PAR. Agric For Meteorol 100(2–3):103–125
12. Gaastra P (1959) Photosynthesis of crop plants as influenced by light, carbon dioxide, temperature, and stomatal diffusion resistance. Mededel Landbouwhogeschool Wageningen 59:1–68
13. Nichiporovich A (1960) Conference on measurement of visible radiation in plant physiology. Sov Plant Physiol 7:744–747
14. McCree K (1966) A solarimeter for measuring photosynthetically active radiation. Agric Meteorol 3(5–6):353–366, cited By (since 1996) 20
15. Ross J (1975) Radiative transfer in plant communities. In: Monteith JL (ed) Vegetation and the atmosphere, vol 1. Academic, London/New York, pp 13–55

16. ISO (2004) Spatial distribution of daylight. CIE standard general sky. ISO 15469:2004/CIE 011:2003. ISO, 2004
17. LI-COR (1986) LI-COR radiation sensors. instruction manual. Publ. no 8609-56. Lincoln, Nebraska
18. LI-COR (1991) LI-COR radiation measurement instruments. Lincoln, Nebraska
19. Pearcy R (1989) Radiation and light measurements. In: Pearcy R, Ehleringer J, Mooney H, Rundel P (eds) Plant physiological ecology. Chapman & Hall, New York, pp 97–116, ch. 6
20. Ross J, Sulev M, Saarelaid P (1998) Statistical treatment of the PAR variability and its application to willow coppice. Agric For Meteorol 91(1–2):1–21
21. Norman JM, Tanner CB, Thurtell GW (1969) Photosynthetic light sensor for measurements in plant canopies. Agron J 61(6):840–843
22. Britton CM, Dodd JD (1976) Relationships of photosynthetically active radiation and shortwave irradiance. Agric Meteorol 17(1):1–7
23. Howell TA, Meek DW, Hatfield JL (1983) Relationship of photosynthetically active radiation to shortwave radiation in the San-Joaquin Valley. Agric Meteorol 28(2):157–175
24. Alados I, FoyoMoreno I, Alados-Arboledas L (1996) Photosynthetically active radiation: Measurements and modelling. Agric For Meteorol 78(1–2):121–131
25. Fielder P, Comeau P (2000) Construction and testing of an inexpensive PAR sensor. Ministry of Forests Research, British Columbia, Working Paper 53/2000
26. Rodskjer N, Kornher A (1971) Über die bestimmung der strahlungsenergie im wellen-längenbereich von 0, 3–0, 7 [mu] in pflanzenbeständen. Agric Meteorol 8:139–150
27. Slomka J, Slomka K (1986) Participation of photosynthetically active radiation in global radiation. In: Publications of the Institute of Geophysics, Polish Academy of Sciences, p 197
28. Stanhill G, Fuchs M (1977) Relative flux-density of photosynthetically active radiation. J Appl Ecol 14(1):317–322
29. Stigter CJ, Musabilha VMM (1982) The conservative ratio of photosynthetically active to total radiation in the tropics. J Appl Ecol 19(3):853–858
30. Blackburn WJ, Proctor JTA (1983) Estimating photosynthetically active radiation from measured solar irradiance. Sol Energy 31(2):233–234
31. Hansen V (1984) Spectral distribution of solar-radiation on clear days - a comparison between measurements and model estimates. J Climate Appl Meteorol 23(5):772–780
32. Rao CRN (1984) Photosynthetically active components of global solar-radiation – measurements and model computations. Arch Meteorol Geophys Bioclimatol B Theor Appl Climatol 34(4):353–364
33. Spitters CJT, Toussaint HAJM, Goudriaan J (1986) Separating the diffuse and direct component of global radiation and its implications for modeling canopy photosynthesis. 1. components of incoming radiation. Agric For Meteorol 38(1–3):217–229
34. Tooming H, Niilisk H (1967) Transition coefficients from integrated radiation to photosynthetic active radiation (PAR) under field conditions. In: Phytoactinometrical investigations of plant canopy (in Russian). Valgus Publishers, Tallinn, pp 140–149
35. Karalis JD (1989) Characteristics of direct photosynthetically active radiation. Agric For Meteorol 48(3–4):225–234
36. Jacovides CP, Kallos GB, Steven MD (1993) Spectral band resolution of solar-radiation in Athens, Greece. Int J Climatol 13(6):689–697
37. Stephens K, Strickland JDH (1962) Use of a thermopile radiometer for measuring the attenuation of photosynthetically active radiation in the sea. Limnol Oceanogr 7(4):485–487
38. Mims FM (2003) A 5-year study of a new kind of photosynthetically active radiation sensor. Photochem Photobiol 77(1):30–33
39. Mõttus M, Ross J, Sulev M (2001) Experimental study of ratio of PAR to direct integral solar radiation under cloudless conditions. Agric For Meteorol 109(3):161–170
40. Grant RH, Heisler GM, Gao W (1996) Photosynthetically-active radiation: Sky radiance distributions under clear and overcast conditions. Agric For Meteorol 82(1–4):267–292
41. Grant R, Heisler G (1997) Obscured overcast sky radiance distributions for ultraviolet and photosynthetically active radiation. J Appl Meteorol 36(10):1336–1345
42. McArthur LJB (2004) Baseline Surface Radiation Network (BSRN) operations manual, version 2.1. Technical Report WMO/TD-No. 879, World Climate Research Programme Baseline Surface Radiation Network. http://www.bsrn.awi.de/fileadmin/user_upload/Home/Publications/McArthur.pdf
43. Michalsky JJ, Harrison LC, Berkheiser WE (1995) Cosine response characteristics of some radiometric and photometric sensors. Sol Energy 54(6):397–402
44. Su WY, Charlock TP, Rose FG, Rutan D (2007) Photosynthetically active radiation from Clouds and the Earth's Radiant Energy System (CERES) products. J Geophys Res Biogeosci 112(G2):G02022
45. BSRN (2005) UV and PAR measurement. Report of the eighth session of the Baseline Surface Radiation Network (BSRN) workshop and scientific review meeting (Exeter, UK, 26–30 July 2004), vol 4/2005, pp 14–16. World Climate Research Programme, Informal Report 4/2005, 2005
46. Gueymard CA (2008) REST2: High-performance solar radiation model for cloudless-sky irradiance, illuminance, and photosynthetically active radiation – validation with a benchmark dataset. Sol Energy 82(3):272–285
47. Alados I, Alados-Arboledas L (Jan 1999) Direct and diffuse photosynthetically active radiation: measurements and modelling. Agric For Meteorol 93:27–38
48. Bosch JL, Lopez G, Batlles FJ (Jan 2009) Global and direct photosynthetically active radiation parameterizations for clear-sky conditions. Agric For Meteorol 149:146–158
49. Perez R, Ineichen P, Seals R, Michalsky J, Stewart R (1990) Modeling daylight availability and irradiance components from direct and global irradiance. Sol Energy 44(5):271–289
50. Alados I, Olmo FJ, Foyo-Moreno I, Alados-Arboledas L (Apr 2000) Estimation of photosynthetically active radiation under cloudy conditions. Agric For Meteorol 102:39–50

51. Alados-Arboledas L, Olmo FJ, Alados I, Perez M (2000) Parametric models to estimate photosynthetically active radiation in Spain. Agric For Meteorol 101(2–3):187–201
52. Jacovides CP, Timbios F, Asimakopoulos DN, Steven MD (1997) Urban aerosol and clear skies spectra for global and diffuse photosynthetically active radiation. Agric For Meteorol 87(2–3):91–104
53. Papaioannou G, Papanikolaou N, Retalis D (1993) Relationships of photosynthetically active radiation and shortwave irradiance. Theor Appl Climatol 48(1):23–27
54. Jacovides CP, Tymvios FS, Asimakopoulos DN, Theofilou KM, Pashiardes S (2003) Global photosynthetically active radiation and its relationship with global solar radiation in the Eastern Mediterranean basin. Theor Appl Climatol 74(3–4):227–233
55. Wang Q, Kakubari Y, Kubota M, Tenhunen J (Jan 2007) Variation on PAR to global solar radiation ratio along altitude gradient in Naeba Mountain. Theor Appl Climatol 87:239–253
56. McCree K (1981) Photosynthetically active radiation. In: Pirson A, Zimmermann M (eds) Encyclopedia of plant physiology, vol 12A. Springer, Berlin, Heidelberg, pp 41–55
57. Dye DG (2004) Spectral composition and quanta-to-energy ratio of diffuse photosynthetically active radiation under diverse cloud conditions. J Geophys Res Atmos 109(D10): D10203
58. Kirk JTO (1994) Light and photosynthesis in aquatic ecosystems, 2nd edn. Cambridge University Press, Cambridge/ England
59. Buiteveld H, Hakvoort JH, Donze M (Oct 1994) Optical properties of pure water. In: Jaffe JS (ed) Society of Photo-Optical Instrumentation Engineers (SPIE) conference series, vol 2258 of Society of Photo-Optical Instrumentation Engineers (SPIE) Conference Series, pp 174–183
60. Bricaud A, Babin M, Morel A, Claustre H (1995) Variability in the chlorophyll-specific absorption-coefficients of natural phytoplankton - analysis and parameterization. J Geophys Res Oceans 100(C7):13321–13332
61. Bricaud A, Stramski D (1990) Spectral absorption-coefficients of living phytoplankton and nonalgal biogenous matter - a comparison between the Peru upwelling area and the Sargasso sea. Limnol Oceanogr 35(3):562–582
62. Jerlov NG (1976) Marine optics. Elsevier, Amsterdam/New York
63. Austin RW, Petzold TJ (1986) Spectral dependence of the diffuse attenuation coefficient of light in ocean waters. Opt Eng 25(3):471–479
64. Reinart A, Herlevi A (1999) Diffuse attenuation coefficient in some Estonian and Finnish lakes. Proc Estonian Acad Sci Biol Ecol 48(4):267–283
65. Reinart A, Arst H, Blanco-Sequeiros A, Herlevi A (1998) Relation between underwater irradiance and quantum irradiance in dependence on water transparency at different depths in the water bodies. J Geophys Res Oceans 103(C4):7749–7752
66. Dera J (1992) Marine physics. Elsevier, Amsterdam
67. Ehn J, Granskog MA, Reinart A, Erm A (2004) Optical properties of melting land-fast sea ice and underlying seawater in Santala Bay, Gulf of Finland. J Geophys Res Oceans 109(C9):C09003
68. Morel A, Smith RC (1974) Relation between total quanta and total energy for aquatic photosynthesis. Limnol Oceanogr 19(4):591–600
69. Aas E (1971) Natural history of Hardangerfjord. 9. Irradiance in Hardangerfjorden 1967. Sarsia 46:59–78
70. Ohmura A, Dutton EG, Forgan B, Frohlich C, Gilgen H, Hegner H, Heimo A, Konig-Langlo G, McArthur B, Muller G, Philipona R, Pinker R, Whitlock CH, Dehne K, Wild M (1998) Baseline surface radiation network (BSRN/WCRP): New precision radiometry for climate research. Bull Am Meteorol Soc 79(10):2115–2136
71. Baldocchi D, Falge E, Gu LH, Olson R, Hollinger D, Running S, Anthoni P, Bernhofer C, Davis K, Evans R, Fuentes J, Goldstein A, Katul G, Law B, Lee XH, Malhi Y, Meyers T, Munger W, Oechel W, Paw KT, Pilegaard K, Schmid HP, Valentini R, Verma S, Vesala T, Wilson K, Wofsy S (2001) FLUXNET: A new tool to study the temporal and spatial variability of ecosystem-scale carbon dioxide, water vapor, and energy flux densities. Bull Am Meteorol Soc 82(11):2415–2434
72. Friend AD, Arneth A, Kiang NY, Lomas M, Ogee J, Rodenbeckk C, Running SW, Santaren JD, Sitch S, Viovy N, Woodward FI, Zaehle S (2007) FLUXNET and modelling the global carbon cycle. Glob Change Biol 13(3):610–633
73. Augustine JA, DeLuisi JJ, Long CN (2000) SURFRAD - a national surface radiation budget network for atmospheric research. Bull Am Meteorol Soc 81(10):2341–2357
74. Hari P, Andreae MO, Kabat P, Kulmala M (2009) A comprehensive network of measuring stations to monitor climate change. Boreal Environ Res 14(4):442–446
75. Jacquemoud S, Baret F (1990) Prospect - a model of leaf optical-properties spectra. Remote Sens Environ 34(2):75–91
76. Feret JB, Francois C, Asner GP, Gitelson AA, Martin RE, Bidel LPR, Ustin SL, le Maire G, Jacquemoud S (2008) PROSPECT-4 and 5: Advances in the leaf optical properties model separating photosynthetic pigments. Remote Sens Environ 112(6):3030–3043
77. Sims DA, Gamon JA (2002) Relationships between leaf pigment content and spectral reflectance across a wide range of species, leaf structures and developmental stages. Remote Sens Environ 81(2–3):337–354
78. Martin G, Josserand SA, Bornman JF, Vogelmann TC (1989) Epidermal focusing and the light microenvironment within leaves of medicago-sativa. Physiol Plant 76(4):485–492
79. Farquhar GD, Caemmerer SV, Berry JA (1980) A biochemical-model of photosynthetic CO2 assimilation in leaves of C-3 species. Planta 149(1):78–90
80. Tardieu F, Simonneau T (1998) Variability among species of stomatal control under fluctuating soil water status and evaporative demand: modelling isohydric and anisohydric behaviours. J Exp Bot 49:419–432
81. Emerson R (1929) The relation between maximum rate of photosynthesis and concentration of chlorophyll. J Gen Physiol 12(5):609–622
82. Peñuelas J, Baret F, Filella I (1995) Semiempirical indexes to assess carotenoids chlorophyll-a ratio from leaf spectral reflectance. Photosynthetica 31(2):221–230

83. Moya I, Camenen L, Evain S, Goulas Y, Cerovic ZG, Latouche G, Flexas J, Ounis A (2004) A new instrument for passive remote sensing 1, measurements of sunlight-induced chlorophyll fluorescence. Remote Sens Environ 91(2):186–197
84. Maxwell K, Johnson GN (2000) Chlorophyll fluorescence - a practical guide. J Exp Bot 51(345):659–668
85. Ross J (1981) The radiation regime and architecture of plant stands. Dr. W. Junk Publishers, The Hague
86. Myneni R, Ross JE (1991) Photon-vegetation interactions. Springer, Berlin, Heidelberg
87. Malenovsky Z, Mishra KB, Zemek F, Rascher U, Nedbal L (2009) Scientific and technical challenges in remote sensing of plant canopy reflectance and fluorescence. J Exp Bot 60(11): 2987–3004
88. Monsi M, Saeki T (1953) Über den lichtfaktor in den pflanzengesellschaften und seine bedeutung für die stoffproduktion. Jpn J Bot 14:22–52
89. Monsi M, Saeki T (2005) On the factor light in plant communities and its importance for matter production. Ann Bot 95(3):549–567
90. Lieffers V, Messier C, Stadt K, Gendron F, Comeau P (1999) Predicting and managing light in the understory of boreal forests. Can J For Res 29(6):796–811
91. Campbell GS, Norman JM (1998) Introduction to environmental biophysics, 2nd edn. Springer, New York
92. Breda NJJ (Nov 2003) Ground-based measurements of leaf area index: a review of methods, instruments and current controversies. J Exp Bot 54:2403–2417
93. Jonckheere I, Fleck S, Nackaerts K, Muys B, Coppin P, Weiss M, Baret F (Jan 2004) Review of methods for in situ leaf area index determination - Part I theories, sensors and hemispherical photography. Agric For Meteorol 121:19–35
94. Ni WG, Li XW, Woodcock CE, Roujean JL, Davis RE (Dec 1997) Transmission of solar radiation in boreal conifer forests: Measurements and models. J Geophys Res Atmos 102:29555–29566
95. Mõttus M, Sulev M (2006) Radiation fluxes and canopy transmittance: Models and measurements inside a willow canopy. J Geophys Res Atmos 111(D2):D02109
96. Chelle M (2006) Could plant leaves be treated as Lambertian surfaces in dense crop canopies to estimate light absorption? Ecol Modell 198(1–2):219–228
97. Asner GP, Wessman CA, Schimel DS, Archer S (Mar 1998) Variability in leaf and litter optical properties: Implications for BRDF model inversions using AVHRR, MODIS, and MISR. Remote Sens Environ 63:243–257
98. Baldocchi D, Collineau S (1994) The physical nature of solar radiation in heterogeneous canopies: spatial and temporal attributes. In: Exploitation of environmental heterogeneity by plants: ecophysiological processes above- and below ground. Academic, San Diego, pp 21–71
99. Reifsnyder W, Furnival G, Horowitz J (1971–1972) Spatial and temporal distribution of solar radiation beneath forest canopies. Agric Meteorol 9:21–37
100. DePury DGG, Farquhar GD (May 1997) Simple scaling of photosynthesis from leaves to canopies without the errors of big-leaf models. Plant Cell Environ 20:537–557
101. Oker-Blom P (1985) Photosynthesis of a Scots pine shoot – simulation of the irradiance distribution and photosynthesis of a shoot in different radiation-fields. Agric For Meteorol 34(1):31–40
102. Myneni RB, Asrar G, Wall GW, Kanemasu ET, Impens I (1986) Canopy architecture, irradiance distribution on leaf surfaces and consequent photosynthetic efficiencies in heterogeneous plant canopies. 2 results and discussion. Agric For Meteorol 37(3):205–218
103. Stenberg P (1998) Implications of shoot structure on the rate of photosynthesis at different levels in a coniferous canopy using a model incorporating grouping and penumbra. Funct Ecol 12(1):82–91
104. Gu LH, Baldocchi D, Verma SB, Black TA, Vesala T, Falge EM, Dowty PR (2002) Advantages of diffuse radiation for terrestrial ecosystem productivity. J Geophys Res Atmos 107(D5–6):4050
105. Roderick ML, Farquhar GD, Berry SL, Noble IR (Sept 2001) On the direct effect of clouds and atmospheric particles on the productivity and structure of vegetation. Oecologia 129:21–30
106. Gu LH, Baldocchi DD, Wofsy SC, Munger JW, Michalsky JJ, Urbanski SP, Boden TA (2003) Response of a deciduous forest to the Mount Pinatubo eruption: Enhanced photosynthesis. Science 299(5615):2035–2038
107. Mercado LM, Bellouin N, Sitch S, Boucher O, Huntingford C, Wild M, Cox PM (Apr 2009) Impact of changes in diffuse radiation on the global land carbon sink. Nature 458:1014–1017
108. Vesala T, Markkanen T, Palva L, Siivola E, Palmroth S, Hari P (Feb. 2000) Effect of variations of PAR on CO2 exchange estimation for Scots pine. Agric For Meteorol 100:337–347
109. Schmid HP (1997) Experimental design for flux measurements: matching scales of observations and fluxes. Agric For Meteorol 87(2–3):179–200
110. Schaepman-Strub G, Schaepman ME, Painter TH, Dangel S, Martonchik JV (2006) Reflectance quantities in optical remote sensing-definitions and case studies. Remote Sens Environ 103(1):27–42
111. Nicodemus FE (1970) Reflectance nomenclature and directional reflectance and emissivity. Appl Opt 9(6):1474–1475
112. Baret F, Guyot G (1991) Potentials and limits of vegetation indexes for LAI and APAR assessment. Remote Sens Environ 35(2–3):161–173
113. McCallum I, Wagner W, Schmullius C, Shvidenko A, Obersteiner M, Fritz S, Nilsson S (2010) Comparison of four global FAPAR datasets over Northern Eurasia for the year 2000. Remote Sens Environ 114(5):941–949
114. Asrar G (1989) Theory and applications of optical remote sensing. Wiley, New York
115. Begue A, Desprat JF, Imbernon J, Baret F (1991) Radiation use efficiency of pearl-millet in the Sahelian zone. Agric For Meteorol 56(1–2):93–110
116. Gobron N, Pinty B, Aussedat O, Chen JM, Cohen WB, Fensholt R, Gond V, Huemmrich KF, Lavergne T, Melin F,

Privette JL, Sandholt I, Taberner M, Turner DP, Verstraete MM, Widlowski JL (2006) Evaluation of fraction of absorbed photosynthetically active radiation products for different canopy radiation transfer regimes: methodology and results using joint research center products derived from SeaWiFS against ground-based estimations. J Geophys Res Atmos 111(D13110):1–15

117. Russel G, Jarvis P, Monteith J (1989) Absorption of radiation by canopies and stand growth. In: Russel G, Marshall B, Jarvis PG (eds) Plant canopies: their growth, form and function. Cambridge University Press, New York, pp 21–39
118. Palva L, Garam E, Manoochehri F, Sepponen R, Hari P, Rajala K, Ruotoistenmaki H, Seppala I (1998) A novel multipoint measuring system of photosynthetically active radiation. Agric For Meteorol 89(2):141–147
119. Palva L, Markkanen T, Siivola E, Garam E, Linnavuo M, Nevas S, Manoochehri F, Palmroth S, Rajala K, Ruotoistenmaki H, Vuorivirta T, Seppala I, Vesala T, Hari P, Sepponen R (2001) Tree scale distributed multipoint measuring system of photosynthetically active radiation. Agric For Meteorol 106(1):71–80
120. Baret F, Hagolle O, Geiger B, Bicheron P, Miras B, Huc M, Berthelot B, Nino F, Weiss M, Samain O, Roujean JL, Leroy M (2007) LAI, fAPAR and fCover CYCLOPES global products derived from VEGETATION - part 1: Principles of the algorithm. Remote Sens Environ 110(3):275–286
121. Chen JM (1996) Optically-based methods for measuring seasonal variation of leaf area index in boreal conifer stands. Agric For Meteorol 80(2–4):135–163
122. Nilson T (1971) Theoretical analysis of frequency of gaps in plant stands. Agric Meteorol 8(1):25–38
123. Lang ARG (1986) Leaf-area and average leaf angle from transmission of direct sunlight. Aust J Bot 34(3):349–355
124. Welles JM, Norman JM (1991) Instrument for indirect measurement of canopy architecture. Agron J 83:818–825
125. Baret F, Andrieu B, Folmer J, Hanocq J, Sarrouy C (1993) Gap fraction measurement from hemispherical infrared photography and its use to evaluate PAR interception efficiency. In: Crop structure and microclimate: characterization and applications, INRA edn. Paris, pp 359–372
126. Leblanc SG, Chen JM, Fernandes R, Deering DW, Conley A (2005) Methodology comparison for canopy structure parameters extraction from digital hemispherical photography in boreal forests. Agric For Meteorol 129:187–207
127. Cescatti A (2007) Indirect estimates of canopy gap fraction based on the linear conversion of hemispherical photographs: Methodology and comparison with standard thresholding techniques. Agric For Meteorol 143:1–12
128. Lang M, Kuusk A, Mõttus M, Rautiainen M, Nilson T (2010) Canopy gap fraction estimation from digital hemispherical images using sky radiance models and a linear conversion method. Agric For Meteorol 150(1):20–29
129. Campbell GS (1986) Extinction coefficients for radiation in plant canopies calculated using an ellipsoidal inclination angle distribution. Agric For Meteorol 36(4):317–321
130. Asrar G, Fuchs M, Kanemasu ET, Hatfield JL (1984) Estimating absorbed photosynthetic radiation and leaf-area index from spectral reflectance in wheat. Agron J 76(2):300–306
131. Myneni RB, Williams DL (1994) On the relationship between fAPAR and NDVI. Remote Sens Environ 49(3):200–211
132. Weiss M, Baret F (1999) Evaluation of canopy biophysical variable retrieval performances from the accumulation of large swath satellite data. Remote Sens Environ 70(3):293–306
133. Weiss M, Baret F, Myneni RB, Pragnere A, Knyazikhin Y (2000) Investigation of a model inversion technique to estimate canopy biophysical variables from spectral and directional reflectance data. Agronomie 20(1):3–22
134. Roujean JL, Breon FM (1995) Estimating PAR absorbed by vegetation from bidirectional reflectance measurements. Remote Sens Environ 51(3):375–384
135. Myneni RB, Hoffman S, Knyazikhin Y, Privette JL, Glassy J, Tian Y, Wang Y, Song X, Zhang Y, Smith GR, Lotsch A, Friedl M, Morisette JT, Votava P, Nemani RR, Running SW (2002) Global products of vegetation leaf area and fraction absorbed PAR from year one of MODIS data. Remote Sens Environ 83(1–2):214–231
136. Bacour C, Baret F, Beal D, Weiss M, Pavageau K (2006) Neural network estimation of LAI, fAPAR, fCover and LAIxC(ab), from top of canopy MERIS reflectance data: Principles and validation. Remote Sens Environ 105(4):313–325
137. Fensholt R, Sandholt I, Rasmussen MS (2004) Evaluation of MODIS LAI, fAPAR and the relation between fAPAR and NDVI in a semi-arid environment using in situ measurements. Remote Sens Environ 91(3–4):490–507
138. Morisette JT, Baret F, Privette JL, Myneni RB, Nickeson JE, Garrigues S, Shabanov NV, Weiss M, Fernandes RA, Leblanc SG, Kalacska M, Sanchez-Azofeifa GA, Chubey M, Rivard B, Stenberg P, Rautiainen M, Voipio P, Manninen T, Pilant AN, Lewis TE, Iiames JS, Colombo R, Meroni M, Busetto L, Cohen WB, Turner DP, Warner ED, Petersen GW, Seufert G, Cook R (2006) Validation of global moderate-resolution LAI products: A framework proposed within the CEOS Land Product Validation subgroup. IEEE Trans Geosci Remote Sens 44(7):1804–1817
139. Weiss M, Baret F, Garrigues S, Lacaze R (2007) LAI and fAPAR CYCLOPES global products derived from VEGETATION, part 2: validation and comparison with MODIS collection 4 products. Remote Sens Environ 110(3):317–331
140. Wiegand CL, Maas SJ, Aase JK, Hatfield JL, Pinter PJ, Jackson RD, Kanemasu ET, Lapitan RL (1992) Multisite analyses of spectral-biophysical data for wheat. Remote Sens Environ 42(1):1–21
141. Sellers PJ (1985) Canopy reflectance, photosynthesis and transpiration. Int J Remote Sens 6(8):1335–1372
142. Baret F, Pavageau K, Béal D, Weiss M, Berthelot B, Regner P (2006) Algorithm theoretical basis document for MERIS top of atmosphere land products (TOA_VEG). INRA-CSE, 2006
143. Deng F, Chen JM, Plummer S, Chen MZ, Pisek J (2006) Algorithm for global leaf area index retrieval using satellite imagery. IEEE Trans Geosci Remote Sens 44(8):2219–2229

144. Baret F, Weiss M, Lacaze R, Camacho F, Pacholcyzk P, Makhmara H, Smets B (2010) Consistent and accurate LAI, FAPAR and FCOVER global products: principles and evaluation of GEOV1 products. In Sobrino (ed) Proceedings of the third international symposium on recent advances in quantitative remote sensing, Valencia (Spain), pp 208–213

Photovoltaic Energy, Introduction

Daniel Lincot
Institute of Research and Development of Photovoltaic Energy, Chatou, Cedex, France

Article Outline

Glossary

III-V Solar cells Solar cells based on compound combining elements from the Ga and As columns (III and V).

Cadmium telluride (CdTe) solar cells Solar cells based on this compound, used in the form of thin films.

Chalcopyrite solar cells Solar cells based on the compound $Cu(In,Ga)Se_2$, also noted CIGS, in the form of thin films.

Dye sensitized solar cells (DSSC) Solar cells based on mesoscopic tintanium oxide thin film sensitized with dye photoactive molecules and impregnated by an electrolyte.

Hot carrier solar cell New high efficiency concept allowing to convert high energy photons in electrical charges in the external circuit without thermal losses.

Life cycle analysis (LCA) To quantify all the steps from mining, utilization to recycling in terms of energy consumption, material utilization, environmental and health impacts.

Multijunction solar cell High efficiency solar cell based on the association of several elementary solar cells made of sing junctions.

Organic solar cells Solar cells based on organic components like carbon fullerenes and polymers, blended in the form of thin films.

Pay back time Time needed by a solar cell under operation to reimburse the total energy used for its fabrication.

Photovoltaics Conversion of photon energy to electricity.

Siicon solar cells Solar cells based on silicon element, either in crystalline or amorphous forms.

Solar cells Device allowing to absorb photon energy and convert it to electricity in an external circuit.

Up, down conversion New high efficiency concept using optical processes allowing to convert low (resp. high) energy photons to medium visible energy photons for maxium conversion efficiency.

Photovoltaics is the direct conversion of solar energy into electricity. It results from the fundamental mechanism of absorption of photons in matter, with the excitation of electrons from their equilibrium lower energy state to a nonequilibrium excited state of higher energy. That means that electrons are being transferred to more negative electrical potential. Then, they usually return to equilibrium by giving back the initial photon energy in form of thermal energy (with the interactions with phonons), light with the emission of new photons via luminescence processes or chemical species via electrochemical oxydo reduction processes in the case of photosynthesis. The uniqueness and beauty of photovoltaics is to "plug" on the initial step when electrons are just excited to a lower potential, and to have them directly transferred in an external circuit where the energy can be used directly in the electrical form. The device to do it is just a solar cell. However, to have it efficient imposes to be able to compete with the naturally occurring spontaneous processes! This was not easy and from the discovery of the photovoltaic effect in 1839 by Edmond Becquerel to the first efficient silicon solar cell in 1954 it took more than one century and then 50 years more to reach the years 2000s to assist to the large scale industrial endeavor of photovoltaic conversion of solar energy, bringing for the first time in the human history this new renewable energy technology as an alternative to fossil fuels and nuclear utilizations. While laboratory record efficiency for any photovoltaic cells is reaching the incredible value of 43%, approaching the 50% level, more than 20 GW of photovoltaic peak power sources have been produced by the industry in 2010. This is the